Polysaccharide-Based Theranostic Systems for Combined Imaging and Cancer Therapy Recent Advances and Challenges

Gupta, Aastha; Sood, Ankur; Fuhrer, Erwin; Djanashvili, Kristina; Agrawal, Garima

DOI
10.1021/acsbiomaterials.1c01631

Publication date
2022

Document Version
Final published version

Published in
ACS Biomaterials Science and Engineering

ACS Biomaterials SCIENCE & ENGINEERING

pubs.acs.org/journal/abseba

Review

Polysaccharide-Based Theranostic Systems for Combined Imaging and Cancer Therapy: Recent Advances and Challenges

Aastha Gupta,[⊥] Ankur Sood,[⊥] Erwin Fuhrer,[⊥] Kristina Djanashvili,[⊥] and Garima Agrawal*

Cite This: *ACS Biomater. Sci. Eng.* 2022, 8, 2281−2306

Read Online

ACCESS | Metrics & More | Article Recommendations

ABSTRACT: Designing novel systems for efficient cancer treatment and improving the quality of life for patients is a prime requirement in the healthcare sector. In this regard, theranostics have recently emerged as a unique platform, which combines the benefits of both diagnosis and therapeutics delivery. Theranostics have the desired contrast agent and the drugs combined in a single carrier, thus providing the opportunity for real-time imaging to monitor the therapy results. This helps in reducing the hazards related to treatment overdose or underdose and gives the possibility of personalized therapy. Polysaccharides, as natural biomolecules, have been widely explored to develop theranostics, as they act as a matrix for simultaneously loading both contrast agents and drugs for their utility in drug delivery and imaging. Additionally, their remarkable physicochemical attributes (biodegradability, satisfactory safety profile, abundance, and diversity in functionality and charge) can be tuned via postmodification, which offers numerous possibilities to develop theranostics with desired characteristics. Hence, we provide an overview of recent advances in polysaccharide matrix-based theranostics for drug delivery combined with magnetic resonance imaging, computed tomography, positron emission tomography, single photon emission computed tomography, and ultrasound imaging. Herein, we also summarize the toxicity assessment of polysaccharides, associated contrast agents, and nanotoxicity along with the challenges and future research directions.

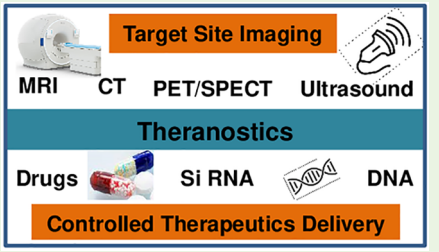

KEYWORDS: *Polysaccharides, Theranostics, Drug delivery, Imaging, Contrast agent, Toxicity*

1. INTRODUCTION

Cancer is one of the most devastating diseases, and the number of cancer patients is increasing globally every year.[1] The effective way of addressing this disease requires an early diagnosis-based treatment. To achieve this, scientists have made enormous efforts in recent years to develop various strategy-based nanomedicines by utilizing the concepts of modern nanotechnology.[2,3] In this regard, significant attention has been given to developing theranostics, which are basically nanosystems that can achieve imaging combined with therapeutics delivery (Figure 1).[4] After the inception of this term "theranostics" in the 2000s by Funkhouser, this area has seen tremendous development in the last two decades.[5]

In this context, a variety of synthetic polymers such as polyethylene glycol (PEG), polyvinylcaprolactam (PVCL), polycaprolactone (PCL), poly(lactic acid) (PLA), poly(lactic-*co*-glycolic acid) (PLGA), and poly(acrylic acid) (PAA) have been explored for designing nanocarriers for cancer therapy.[6−10] The use of synthetic polymers gives us the possibility of controlling the molecular weight, mechanical properties, chemical functionality, and reproducibility.[11,12] On the other hand, natural polymers such as polysaccharides have gained rapidly growing interest, as they provide the advantages of inherent biocompatibility, biodegradability, and nonimmunogenicity, which are crucial for developing efficient theranostic systems.[13,14] To achieve the targeted physicochemical properties with high efficiency, these polysaccharides can be further modified by chemical functionalization.[15−18] Additionally, various natural and synthetic polymers have also been combined via grafting techniques resulting in a hybrid polymer matrix for designing theranostic systems.[19,20]

Further, to obtain a theranostic system capable of drug delivery and imaging, various imaging agents including metal nanoparticles, small molecule complex, radioactive agents, and micro/nanobubbles have been explored in combination with natural polymer-based nanocarriers.[21] Based on the properties of the imaging agent used, the developed theranostic system can be utilized for different imaging modalities such as magnetic resonance imaging (MRI), computed tomography (CT), positron emission tomography (PET), single photon emission computed tomography (SPECT), and ultrasound imaging.

Received: December 28, 2021
Accepted: April 20, 2022
Published: May 5, 2022

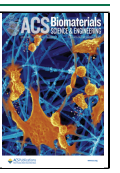

https://doi.org/10.1021/acsbiomaterials.1c01631
ACS Biomater. Sci. Eng. 2022, 8, 2281−2306

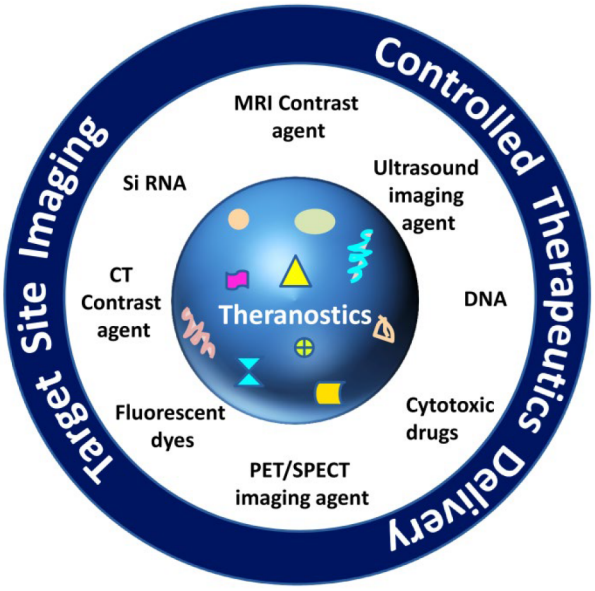

Figure 1. Schematic representation of theranostic system involving combined therapeutics delivery and imaging.

A number of articles have been reported in the literature that discuss the fundamentals of theranostics and various polymeric systems mainly based on synthetic polymers.[22,23] However, very little attention has been paid to polysaccharide-based matrixes for designing theranostic systems. The review articles from Jaymand et al. and Swierczewska et al. describe the structure and physicochemical properties of different polysaccharides and how they can be modified for developing theranostic systems.[24,25] However, a comprehensive overview of their use as a biopolymer matrix for theranostic systems is missing. To the best of our knowledge based on the careful observation of literature articles, this is a timely comprehensive review describing the recent advancement in the use of polysaccharide-based matrixes with nanomaterials for single/multimodal imaging techniques (e.g., MRI, CT, PET/SPECT, and ultrasound imaging) combined with drug delivery. Apart from providing the readers with a brief overview of various contrast agents used in these imaging methods, we also discuss the toxicity issue related to the contrast agents and different challenges that need to be overcome to ensure the successful commercial application of currently lab-scale theranostic systems.

2. TECHNICAL SPECIFICATIONS OF IMAGING SYSTEMS WITH CONTRAST AGENTS

2.1. MRI and Contrast Agents. *2.1.1. Contrast Concepts in MRI.* The signal obtained in standard clinical MRI is based on the availability of abundant protons in the tissue. Spatial encoding is obtained by controlled superposition of short-time weak magnetic fields produced by coils featuring a linear spatial gradient. The typical MRI sound arises from switching these coils to produce these intermittent weak magnetic fields. This yields a position-dependent frequency shift of spatially distributed spins which can be used to extract the spatial origin of the signal (data is collected in the so-called *k*-space). There are two major contrast mechanisms which are used extensively in MRI: (i) T_1-weighting and (ii) T_2-weighting. T_1-weighting uses the fact that the longitudinal relaxation (T_1-relaxation) varies significantly among different tissue types. Hence, with a certain timing protocol of excitation and acquisition, a so-called MR sequence, the degree of saturation differs among tissue types. This approach results in signal strength variation among different tissues yielding the desired contrast. T_2-weighting uses the fact that the transverse relaxation time (T_2-relaxation) differs among tissue types. Hence, specific MR sequences have been developed in which the signal strength varies among tissues exhibiting shorter and longer transverse relaxation times. For both MR image types, there is an intrinsic contrast due to different proton contents. MR sequences with no T_1- and T_2-weighting yield pure contrast due to proton density, so-called proton-density weighted images. In the last 30 years, there have been major breakthroughs in developing further MR sequences which facilitate the application of more advanced contrast mechanisms. Few examples are the visualization of flow (flow MRI),[26] contrast due to diffusion mechanisms (diffusion weighted imaging (DWI) and diffusion tensor imaging (DTI)),[27] MR thermometry to measure temperature,[28] and, probably most famous, functional MRI (fMRI) which builds up contrast due to blood-oxygen-level-dependence (BOLD) and enables the visualization of active brain areas.[29] In summary, MRI contains manifold intrinsic contrast mechanisms; yet there are two main types of contrast agents with applications in medical diagnostics. The contrast agents can be classified by their ability to change the relaxation rates $R_1 = 1/T_1$ and $R_2 = 1/T_2$, which leads to the definition of r_1 for the longitudinal relaxivity and r_2 for the transverse relaxivity.[30] The effect of a contrast agent to change the immanent relaxation of a target tissue is given by eq 1[31]

$$\frac{1}{T_i} = \frac{1}{T_i^0} + r_i \times [\mathrm{CA}] \tag{1}$$

$(1/T_i^0)$ describes the immanent relaxation of a tissue, whereas $(1/T_i)$ describes the relaxation rate when a contrast agent is present. The relaxivity r_i of a contrast agent is expressed in units of $\mathrm{mM}^{-1}\ \mathrm{s}^{-1}$ and [CA] describes the concentration of the contrast agent. A brief introduction to T_1- and T_2-contrast agents is given in the next section.

2.1.2. Contrast Agents in MR. T_1-Contrast Agents. T_1-relaxation describes the return of the spin ensemble after an excitation pulse into its initial state or thermal equilibrium, respectively. The speed of this process depends on the molecular motion and is highly efficient when the molecular tumbling rate has good matching with the Larmor frequency. Hence, T_1-relaxation time depends on the molecular size as well as on the field strength of the static magnetic field. T_1-relaxation speeds up dramatically in the presence of paramagnetic impurities, which means for molecules with unpaired electrons. Often used paramagnetic substances are ion complexes of gadolinium (Gd), manganese (Mn), or dysprosium (Dy).[32] Out of these three options, Gd is the most frequently applied element. In smaller concentrations and thus of less toxicity, Gd has larger longitudinal relaxivity r_1. Areas that have accumulated larger concentrations of Gd appear bright in T_1-weighted images because of the large signal caused by short T_1 relaxation. This effect is used to develop molecular biomarkers that specifically target certain tissues, for example, cancer tissue.[33] These contrast agents are called positive contrast agents.

T_2-Contrast Agents. T_2-relaxation describes the decoherence of the spin ensemble after an excitation pulse and thus the

https://doi.org/10.1021/acsbiomaterials.1c01631
ACS Biomater. Sci. Eng. 2022, 8, 2281−2306

decay of the MR signal. The shorter the decoherence time of a certain tissue type, the less signal is acquired after a certain waiting time (echo time = TE). As a rule of thumb, we can state that T_2-relaxation time increases with molecular tumbling, which means that unbound small molecules have long relaxation times. This explains the T_2-relaxation of water in the range of seconds. The main source of decoherence is dipole−dipole interactions. Due to the relatively larger gyromagnetic ratio of electrons compared to protons, electron−proton interactions are more powerful in inducing T_2 relaxation than proton−proton interactions. Therefore, molecules with unpaired electrons, which are paramagnetic materials, are the main source for T_2 contrast agents.

The most common T_2-contrast agents are superparamagnetic iron-oxide nanoparticles (SPIONPs). In applications for clinical MRI, these particles are embedded in ligands.[30,34] T_2-contrast agents exhibit a negative contrast effect. This means that the regions where contrast agents accumulate appear dark because the rapid T_2 relaxation inhibits the emission of signals from these regions. Current research in the field of developing T_2 contrast agent development investigates the application of metal-alloy particles and magnetosomes. Because of their biological origin, magnetosomes are of particular interest in developing contrast agents, as they promise a high degree of biocompatibility.[35]

Hyperpolarization. Another option in MRI to increase signal in general is to use the effect of hyperpolarization. The net magnetization is drastically enhanced due to non-equilibrium spin polarization. This approach makes it possible to obtain signals from polarizable substances such as Xenon gases. Xenon-enhanced imaging has important applications in lung function analysis.[36,37]

2.2. CT and Contrast Agents. *2.2.1. Contrast Concepts in CT.* Computed tomography (CT) is the most commonly applied noninvasive imaging method in the daily clinical routine for the diagnosis of various diseases, since it is faster and less expensive compared to other imaging methods such as MRI. The imaging modality of CT makes use of tissue-dependent absorption of X-rays. Spatial encoding is obtained by measuring the absorption of X-rays with different optical paths through the desired object. While a set of parallel-rays or fan-out-rays are simultaneously transmitted through a slice, different angles are obtained by rotating the emitter and detector element around the patient. The raw data enables 2D- and 3D-image reconstructions based on Radon- and Fourier-transformation.[38,39] In a simple model, we can express the attenuation coefficient μ of the X-rays using eq 2[40,41]

$$\mu = \frac{\rho Z^4}{AE^3} \tag{2}$$

In this equation, ρ denotes the mass density of a material, Z the atomic number, A the atomic mass, and E the energy of the X-rays. From here, we can derive some important rules of thumb for the inherent contrast mechanism in CT. Tissue with larger ρ, for example, bone tissue, has approximately twice the density than soft tissue and hence absorbs more X-ray energy due to the higher attenuation coefficient.[42,43] In the realm of CT methodology, the absorption of different tissues is measured in Hounsfield units (HU). The HU coefficient is determined according to eq 3[42]

$$\mathrm{HU} = \frac{\mu_{\mathrm{Tissue}} - \mu_{\mathrm{Water}}}{\mu_{\mathrm{Water}}} \times 1000 \tag{3}$$

Contrast between soft tissue and hard tissue (e.g., bones and teeth with HU ≈ 1000) is generally large enough to provide sufficient contrast-to-noise ratio (CNR) for image analysis. On the other hand, the soft tissue contrast, which is by inherent contrast mechanisms, is most often not satisfactory. For example, many soft tissues have contrast values between 30 and 100 HU, which results in weak contrast between two soft-tissue types. An exceptional case is the lung because the large amount of air within lung tissue yields weaker attenuation compared to the surrounding tissue. Thus, CT, next to conventional X-ray imaging, is the method of choice for lung cancer diagnostics, because there is large contrast between a solid tumor and the surrounding lung tissue.

2.2.2. Contrast Agents in CT. Because inherent soft tissue contrast in CT is weak, contrast agents play an important role in CT imaging. Increased contrast in CT is reached by artificially increasing the absorption of X-rays at the target location. Looking at the simple model of eq 1, we can see that the X-ray absorption is proportional to the fourth power of the atomic number. From this, it is comprehensible that we can achieve large attenuations by establishing an excess of elements with high atomic number at a certain location. Further important properties for a CT contrast agent are sufficiently long tissue retention time, large affinity for the target tissue, solubility, and nontoxicity, and the substance or its metabolites must not accumulate in the body. The largest group of chemical agents for CT contrast agents are based on iodine (Z = 53). A second group of contrast agents are lanthanide-based contrast agents. Here, Gd-based (Z = 64) and Dy-based (Z = 66) contrast agents are of particular interest and are commercially available. These contrast agents are also used to increase T_1-relaxation in MRI (see section 2.1.2) which explains the capability of these elements for use as contrast agents in dual-mode imaging modalities for combined CT/MR-imaging. A third group of CT contrast agents is gold nanoparticles (Z = 79, Au NPs) with an increased contrast-per-unit weight compared to iodine and gadolinium.[44] Au NPs are a promising material due to the high attenuation ratio in combination with the biocompatibility. However, as gold is considered a nontoxic material, the toxicological aspect of Au NPs is still being debated.[45,46] Another potential limitation of Au NPs is the high price which may render Au NPs too expensive for daily clinical use. Alternatives are other metallic contrast agents based on bismuth (Z = 83), tantalum (Z = 73), and platinum (Z = 78),[40] to name a few. One important gas type to enhance CT contrast is Xenon (Z = 54), a gas with good solubility in blood and adipose tissue and the ability to cross the blood-brain barrier. It furthermore finds application in analysis of the lung ventilation system.[47] Due to its application in CT and MRI, Xe may be a candidate for dual use in CT/MRI. A detailed analysis of different CT contrast agents is provided by Lusic et al.[41]

2.3. PET/SPECT Contrast Agents. *2.3.1. Contrast Concepts in PET/SPECT.* In contrast to MRI and CT, the image modalities of PET and SPECT do not have intrinsic contrast mechanisms. Radionuclide tracers are required which are the source of detectable radiation. SPECT uses γ-radiation which is emitted by radioactive decay. In SPECT, a γ-decay is the source for the emission of a single γ-photon. In SPECT imaging, we are interested in the distribution process of a

https://doi.org/10.1021/acsbiomaterials.1c01631
ACS Biomater. Sci. Eng. 2022, 8, 2281−2306

tracer element within the human body. With the aid of γ-ray detectors, the source of activity, and thus the distribution of the target tracer in the body, is monitored. The implementation of a collimator guarantees that only photons perpendicular to the detector surface are registered, which allows the user to trace back the spatial origin of the photon. The measurement is conducted from different angles, and with a similar algorithm as used for CT, a 2D or 3D image can be reconstructed. The drawback of a collimator is the absorption of a large number of photons; thus, the SNR is much weaker compared to CT.

Positron emission tomography (PET) makes use of the β^+-decay. A positron is emitted, which is the antimatter counterpart of an electron. When positron and electron collide, two γ-photons are emitted in opposite directions, which can be detected outside the body. A PET system contains many detectors that are placed in a circular arrangement around the patient. This enables the detection of γ-photons with precise spatial resolution. The arrival of both γ-photons at the specific detector location can be correlated, and the origin of the emission can be reconstructed. In this context, detailed technical information is available in the literature,[48] and details about the application in clinical practice have been reviewed by Bateman.[49] Generally, both techniques have large disadvantages with respect to spatial resolution compared to CT or MRI. However, the consequent analysis of tracer pathways enables the spatiotemporal representation of functional processes. Thus, PET or SPECT is also available as combined devices integrated in CT or MRI scanners (e.g., PET-CT or PET-MRI).

2.3.2. Contrast Agents in PET/SPECT. Tracers for SPECT are radionuclides that have a γ-decay channel. Important parameters are the half-life of the decay channel, the biological half-life, and the metabolomic pathway. Measurements of metabolomic pathways depend on the target molecule in which the tracer is embedded. Commonly used tracers are ^{123}I, ^{111}In, ^{67}Ga, ^{201}Tl, and ^{99}mTc.[50] Of particular interest is ^{99}mTc, because it is easily accessible in daily medical use. It can be derived from ^{99} Mo (which forms a so-called Technetium ^{99}m generator). ^{99}Mo has a half-life of approximately 66 h and can thus be easily transported to remote locations.

Tracers for PET, or PET radionuclides, can be found with low atomic number in isotopes of carbon, nitrogen, oxygen, or fluorine. The most common PET tracers are ^{11}C and ^{18}F.[50] ^{11}C, especially, can easily be used to replace a naturally occurring carbon atom. Since carbon is basically the core element in biology, the replacement of the radio-silent ^{12}C by the active ^{11}C opens a vast range of possible tracer molecules. Since ^{12}C and ^{11}C are chemically equivalent, the measurement molecule does not affect the observed process, which yields an optimal measurement environment. In contrast, ^{18}F is not abundantly available in many molecules. However, it can substitute a hydrogen atom as a bioisosteric replacement without too much perturbation. Detailed analysis of different PET contrast agents can be found in the publication by Pimlott et al.[50]

2.4. Ultrasound Contrast Agents. *2.4.1. Contrast Concepts in Ultrasound.* Compared to the previously discussed technologies, ultrasound is the simplest method with respect to instrumentation. Like MRI and CT, ultrasound has intrinsic contrast mechanisms. The physics of ultrasound is based on wave mechanics. Ultrasound technology uses the transmission of acoustic waves into tissue and the subsequent measurement of reflected waves. Two phenomena are important for reflection: First, different tissues have different wave impedance, which results in partial reflection of the wave at the interface of the adjacent tissues. Second, waves are scattered on little inhomogeneities and scattering bodies within a certain tissue type. If the wave impedance between two tissues differs extremely, then a large portion of the wave is reflected. This is for example the case at the interface of soft tissue and hard tissue or at the interface of soft tissue and air. In this case, a large amount of the wave is reflected. On one hand, we get a large signal from such interfaces; however, the volume behind this interface is obscured, because no energy is transmitted beyond this surface. Scattering depends on the tissue itself and is independent of interfaces. This phenomenon allows us to extract information from volumes between interfaces, e.g., from certain tissues or organs. A tissue with little or no scattering appears black, because there is no reflection and hence no information from this region. For example, blood or cavities filled with liquids appear dark. More technical details about ultrasound imaging are presented by Ortiz et al.[51]

2.4.2. Contrast Agents in Ultrasound. Contrast agents in ultrasound are tailor-made to increase the scattering in a target region. Thus, small inhomogeneities with respect to wave impedance are established in this specific region. To increase the affinity of a contrast agent to accumulate in a target region, active and passive targeting methods have been developed.[52] Furthermore, the mechanical stability of the agent, the transition through capillaries, and physiological inertness are important parameters to characterize a contrast agent.[53] Currently available contrast agents are small spheres composed of a thin shell made from phospholipids, proteins, or polymers and contain different gases. Gases which have been used so far include air, perfluoropropane, perfluorobutane, or sulfur hexafluoride.[53] The diameter of spheres ranges from 1 μm up to 10 μm. There are many applications for contrast enhanced ultrasound imaging such as liver tumors, angiogenesis, or inflammatory disease.[54]

3. POLYSACCHARIDE-BASED THERANOSTICS

Polysaccharides, with a vast chemical assortment, inspire us to utilize their functional diversity. Besides, their extensive use in biomedical applications is conferred with imperative structural features, since they are essential components in biological systems.[55] With the innovations in polymer science, polysaccharides can be engineered as biomedical tools with exclusive structures and distinctive functions. The intrinsic functional moieties associated with polysaccharides can act as attachment sites for therapeutic molecules, targeting ligands, and imaging probes via facile chemical amendments to impart sustained circulation time and site-specificity which are essential features for effective theranostic applications.[56] The recent developments in polysaccharide-based nanomaterials have driven a new trend toward the development of multifunctional systems, which is dedicated in accomplishing theranostics applications with superior therapeutic efficacy, mechanical attributes, and satisfactory toxic profiles.[57,58]

Of late, extensive efforts have been made to develop theranostic systems for imaging guided cancer therapy with high efficiency while avoiding any unwanted side effects. In this regard, different nanomaterials such as metal nanoparticles (NPs), inorganic NPs, magnetic NPs, liposomes, micelles, carbon nanotubes, and quantum dots have been used as imaging agents in designing novel theranostic systems.[59−63]

https://doi.org/10.1021/acsbiomaterials.1c01631
ACS Biomater. Sci. Eng. 2022, 8, 2281−2306

Table 1. Overview of Some Recently Reported Polysaccharide-Based Theranostic Systems

polysaccharides	source of extraction	drugs/imaging agent/modalities	synthesis strategy	properties	ref
Alginate	Gulfweed, seaweed of brown algae	Doxorubicin (DOX)/iron oxide nanoparticles (INPs)/MRI	−COOH group modified to −SH using cystamine; Disulfide cross-linking	High loading efficiency (43%), Co-triggered release behavior, Minimal side effects to normal cells, High toxicity to cancer cells	66
Alginate	Seaweed of brown algae	PEI-coated manganese oxide nanoparticles (PEI-Mn_3O_4 NPs)/ MRI	−COOH group activated for amide bond formation with $-NH_2$ group of PEI-Mn_3O_4 NPs; Double emulsion method	High r_1 relaxivity of 26.12 mM^{-1} s^{-1} *in vitro*, Longer circulation time, Cytocompatibility	67
Chitosan		Chitosan coated INPs/MRI	Ionic cross-linking of oleic acid coated INPs with chitosan	Enhanced ROS activity, Upregulation of γH2AX, p53 and, p21 in the presence of blue light, T_2 contrast property	68
Pectin	Citrus	Curcumin/gold coated INPs/MRI	$-NH_2$ group modified to −SH using mercaptopropanoic acid; Gold−thiol chemistry	30% viability for HeLa cells, Enhanced ROS generation under γ-irradiation, r_2 relaxivity in the range of 11.06−13.94 s^{-1} μg^{-1} mL *in vitro*	69
Alginate	Seaweed of brown algae	Curcumin/gold coated INPs/MRI	−COOH group modified to −SH using L-cysteine; Gold−thiol chemistry	Core−shell NPs of around 8.1 nm loading efficiency of 7.2 wt %	70
Dextran	Lactic acid bacteria	Carboxymethyl dextran coated INPs/MRI	−COOH group bonds with INPs surface; Coprecipitation	One pot synthesis, Utility for functional and structural MRI	71
Dextran	Lactic acid bacteria	Epichlorohydrin (ECH) stabilized dextran coated INPs/MRI	Epoxy group of ECH cross-linking with −OH group of dextran	Internalization by macrophages, Absence of hypersensitivity on pig model, r_2 relaxivity ranging 46.8−207.4 mM^{-1} s^{-1} *in vitro*, r_2* relaxivity ranging 105.8−319.2 mM^{-1} s^{-1} *in vitro*	72
Hyaluronic acid (HA)	Animal tissue	Gadolinium (Gd)-Diethylenetriaminepentaacetic dianhydride(DTPA)-HA/MRI	−OH group of HA and −COOH group of DTPA react via ring opening reaction followed by cross-linking with Gd	r_1 relaxivity of 12.51 mM^{-1} s^{-1} *in vitro*, High resolution of cartilage and lesion MR images	73
HA	Animal tissues	Gd-peptide Dendron-HA/MRI	Azide modified Dendron −Gd complex −COOH modified HA with alkynyl group using 4-(4,6-dimethoxy-1,3,5-triazin-2-yl)-4-methylmorpholinium chloride (DMTMM); Click chemistry	r_1 relaxivity of 7.7 mM^{-1} s^{-1} *in vitro*, Retention of the system at tumor site *in vivo*, High hemocompatibility	74
HA	Animal tissues	Superparamagnetic INPs (SPIONs)-Poly-L-Lysin-HA/MRI	−COOH group of HA reacts with $-NH_2$ group of aminoethyl cholanomide; EDC/NHS Cross-linking	Efficient DNA carrier, Enhanced transfection efficiency	75
Dextran	Lactic acid bacteria	supramolecular amorphous-like iron oxide (SAIO)/MRI	Supramolecular assembly	Relaxivity coefficient ratio of ∼1.2 *in vitro*, Long blood circulation, Satisfactory renal clearance	76
Carboxymethyl cellulose (CMC)	Plant origin	L-dopa/Cobalt−copper doped manganese ferrite (CCMn) nanorods/MRI	CMC coated CCMn nanorods; Simple chemical reaction	r_2 relaxivity of 138.33 mM^{-1} s^{-1} *in vitro*, pH dependent drug release profile	77

https://doi.org/10.1021/acsbiomaterials.1c01631
ACS Biomater. Sci. Eng. 2022, 8, 2281−2306

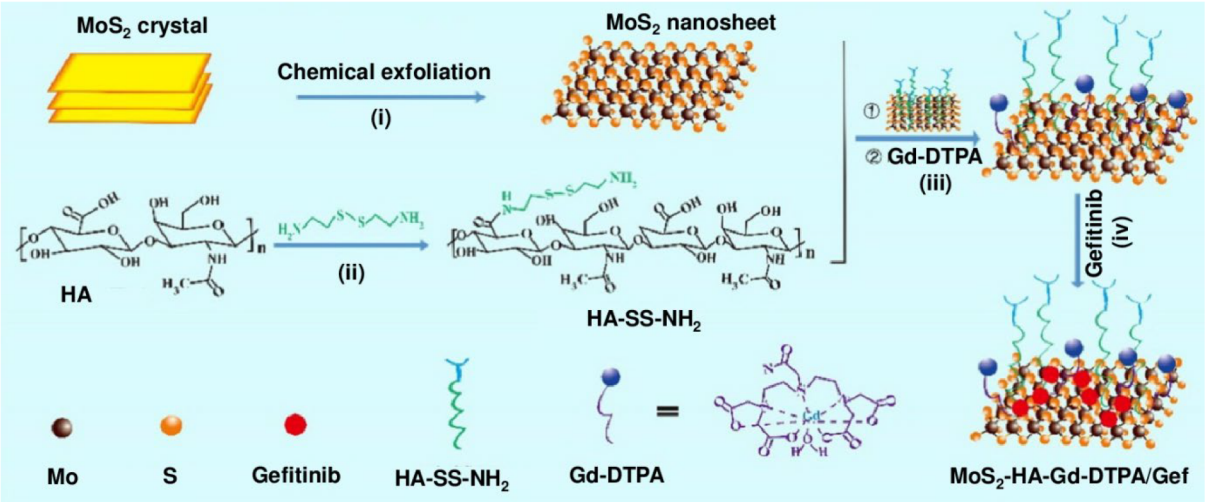

Figure 2. Schematic representation of hyaluronic acid functionalized MoS_2 nanosheets having Gd-DTPA contrast agent and gefitinib drug. Reproduced with permission from ref 83. Copyright 2019 Elsevier Ltd.

These nanomaterials have been combined with various natural polymers such as polysaccharides that act as a carrier matrix in theranostics[24] and cancer immunotherapy.[64] These polymeric matrices help to achieve better solubility and biodistribution of drugs and with renal clearance, crossing biological barriers, and avoiding drug degradation.[65] Additionally, the natural polymer matrix also helps in high drug loading and tuning its release under complex biological conditions. The combination of imaging and drug delivery achieved by these systems helps in anticipating the patient's response to treatment which can be tailored for personalized therapy. Table 1 provides an overview of some recently reported polysaccharide-based theranostic systems with a detailed outline of the fabrication process and key features. Further, in this section, we will discuss various polysaccharides/nanomaterial-based systems for imaging guided cancer therapy.

3.1. Theranostic Systems with MR Imaging Feature. High contrast MR images can be obtained by increasing the r_1 relaxivity of the contrast agent system which in turn is affected by molecular tumbling rate (τ_r).[78,79] The slower the molecular tumbling rate, the higher the r_1 relaxivity will be. To decrease the tumbling rate of complexes used in MRI and to obtain high contrast images, these complexes are conjugated with various polymers which increases the overall molecular weight of the system.[79] Apart from decreasing the molecular tumbling rate, the use of polymer matrix also provides the possibility of loading various drugs to develop multifunctional theranostics.[80]

In this regard, polysaccharide matrix-based theranostics for MR imaging and simultaneous/sequential drug delivery are gaining increasing interest due to low cost of polysaccharides, a variety of available functional groups for post-modification, biocompatibility, biodegradability, and especially higher *in vivo* residence time.[13] This higher residence time is a result of the adhesion of polysaccharide to mucosal surfaces and decreased uptake by phagocytes.[81,82] On the other hand, gadolinium (Gd)-based contrast agents provide positive T_1-weighted MR images but suffer from low relaxivity and short residence time. To address this issue, Gd-based contrast agents have been combined with polysaccharides and nanomaterials. For example, Liu et al. fabricated MoS_2 nanosheets which were decorated with amine-functionalized hyaluronic acid.[83] Next, the diethylenetriaminepentaacetic acid (DTPA) linker was used to load Gd^{3+} ions and combine them with hyaluronic acid functionalized MoS_2 nanosheets. Afterward, an anticancer drug gefitinib was loaded, and the developed system was investigated *in vivo* for its MRI properties. The reported theranostic system was found to have 3.3 times higher relaxivity as compared to commercially available Gd-DTPA contrast agent. Further, the system could effectively convert near-infrared light to heat, causing both a photothermal effect and a release of gefitinib resulting in cell apoptosis in a mouse model having lung cancer (Figure 2). In this way, the developed system could provide the possibility of combining multiple actions including MRI, drug delivery, and photothermal therapy. Further, Cavalli et al. designed chitosan-based nanobubbles (~500 nm) loaded with Gd-DOTP as T_1 MRI contrast agent and prednisolone phosphate as a model drug.[84] A sustained drug release could be achieved by ultrasonic treatment with enhanced T_1 contrast properties owing to the presence of a chitosan shell.

To develop a Gd^{3+}-based safe theranostic system exhibiting no leakage of the contrast agent, Podgorna et al. created Gd^{3+}-loaded alginate nanogels (110 nm) via an inverse mini-emulsion method.[85] The developed nanogels were further modified by using chitosan and alginate via a layer-by-layer technique, and rhodamine B was used as a model drug. The Gd^{3+}-loaded alginate nanogels exhibited reduced T_1 relaxation time. The samples were found to be stable for 2 months with no leaching of Gd^{3+} ions during this time, thus showing their potential for clinically safe theranostics.

To obtain a theranostic system with enhanced T_2 contrast efficiency, Wang et al. explored chitosan modified graphene oxide nanosheets as a single nanocarrier for drug delivery and MR imaging.[86] Herein, chitosan-modified reduced graphene oxide nanosheets were loaded with SPION acting as contrast agent and doxorubicin (DOX) as an anticancer drug. MRI experiments confirmed the potential of the developed system to be used as a T_2 contrast agent with predominant accumulation in cancer cells. Further DOX could also be released under the acidic environment present in cancer cells showing that these SPION and DOX-loaded chitosan-modified reduced graphene oxide nanosheets could be used as an effective theranostic system. In this direction, the drug release

https://doi.org/10.1021/acsbiomaterials.1c01631
ACS Biomater. Sci. Eng. 2022, 8, 2281−2306

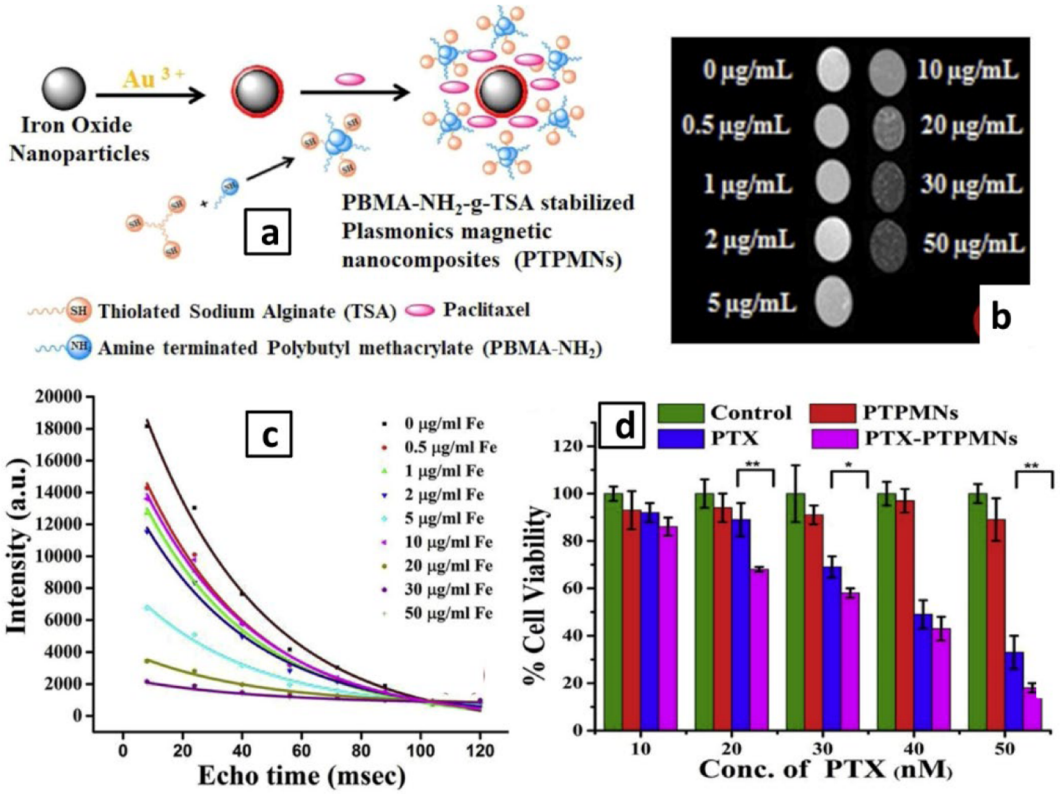

Figure 3. Schematic representation for the fabrication of paclitaxel (PTX)-loaded PTPMNs (a); magnetic resonance images of PTPMNs in phantom gel (b); T_2 relaxation decay curves for PTPMNs (c); cytotoxicity of free PTX, PTPMNs, and PTX loaded PTOMNs against PLC/PRF/5 cells (d). Adapted with permission from ref 89. Copyright 2020 Elsevier Ltd.

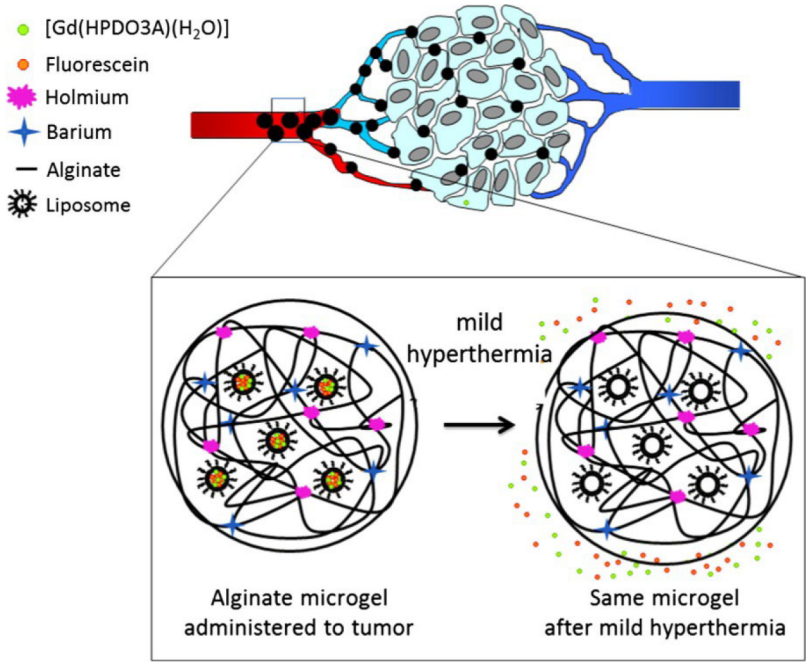

Figure 4. Scheme showing accumulation of alginate microgels in a tumor. Alginate microgels are cross-linked with holmium ions (T_2 MRI agent) and contain temperature-responsive liposomes having fluorescein and [Gd(HPDO3A)(H$_2$O)] as a T_1 MRI contrast agent. In response to temperature (mild hyperthermia), both drug and T_1 contrast agent can be released. Reproduced with permission from ref 90. Copyright 2015 Elsevier Ltd.

efficiency and T_2 contrast efficiency can also be tuned by adjusting the molecular weight of chitosan. Baktash et al. reported that drug delivery could be increased by decreasing the molecular weight of chitosan attached to magnetic

https://doi.org/10.1021/acsbiomaterials.1c01631
ACS Biomater. Sci. Eng. 2022, 8, 2281−2306

graphene oxide nanosheets due to lower hydrogen bonding and $\pi-\pi$ interactions.[87] On the other hand, increasing the molecular weight of chitosan helped in increasing T_2 contrast efficiency by providing efficient coverage of the surface. Similarly, DOX and SPION loaded poly(L-arginine chitosan triphosphate)-based theranostic nanoparticles were developed by Gholami et al. via an ionic gelation method.[88] pH-responsive DOX release was observed achieving the efficient killing of glioblastoma cells. MRI studies confirmed that the increasing iron content in the developed nanoparticles could effectively enhance the T_2 MRI contrast signal. The mentioned studies clearly reveal how the drug release and MR properties of the developed theranostics systems can be tuned by varying different parameters related to both polymer matrix and imaging agent.

Further, taking advantage of the low toxicity of gold-coated Fe_3O_4 nanoparticles reported in the literature, Arora et al. designed plasmonic magnetic nanoparticles decorated with partially modified sodium alginate.[89] Herein, thiolated sodium alginate (TSA) was hydrophobized by grafting amine-functionalized poly(butyl methacrylate) (PBMA). The modified sodium alginate was further used to stabilize gold-coated Fe_3O_4 nanoparticles (PTPMNs). PBMA grafted TSA helped in loading the hydrophobic drug paclitaxel (PTX) with increased loading efficiency (Figure 3a). Loaded drug could be successfully delivered at the target cancer site owing to the breaking of disulfide bonds under the reducing conditions. Additionally, the developed system acted as a negative contrast agent for MRI providing darker images with increasing amounts of iron in the sample (Figure 3b). T_2 decay curves in the iron concentration range 0.5−50 μg/mL exhibited faster relaxation with increasing iron in the phantom gel (Figure 3c). Cytotoxicity experiments demonstrated the higher killing efficiency of PTX loaded PTPMNs as compared to free PTX against PLC/PRF/5 cells (Figure 3d), thus providing the possibility of imaging-guided cancer therapy.[89]

Taking a step further, van Elk et al. fabricated temperature-sensitive liposomes containing alginate microgels to develop a theranostic system capable of performing both T_1 and T_2 MRI along with controlled drug delivery.[90] Here, the liposomes were loaded with fluorescein as a model drug and Prohance [Gd(HPDO3A)(H_2O)] as a T_1 MRI contrast agent. Further, alginate microgels having liposomes were prepared by cross-linking with holmium ions which acted as T_2 MRI contrast agent (Figure 4). The developed system was found to be colloidally stable and could be successfully used for real-time, imaging-guided therapy *in vivo*.

In the quest to develop new theranostic systems, Nejadshafiee et al. developed a magnetic metal organic framework (MOF) nanocomposite-based theranostic system capable of delivering multiple drugs.[91] Herein, magnetic Fe_3O_4 nanoparticles containing MOF with Zn^{2+} ions and curcumin drug were developed. The magnetic MOF nanocomposite was further functionalized with folic acid containing chitosan for targeted delivery and loaded with 5-fluorouracil (5-FU) drug. The developed nanocomposite acted as a robust theranostic system exhibiting controlled release of both curcumin and 5-FU along with enhanced T_2 MRI contrast in cancer cells. To further explore the potential of MOF-based theranostics for multimodal imaging and drug delivery, Lin et al. designed carbon dots embedded MOF@O-carboxymethyl chitosan nanoparticles.[92] The use of *O*-carboxymethyl chitosan in fabricating the particles provided pH-responsive release of doxorubicin. The developed system could be used for dual-imaging including fluorescence and T_2 MRI.

Apart from the contrast agents discussed above, MnO_2 nanomaterials have also gained significant interest for addressing the demand of new theranostic alternatives. For example, Li et al. used a porous coordination network MOF (PCN-224), which in turn was coated with a MnO_2 shell.[93] Further, PCN-224@MnO_2 were loaded with doxorubicin drug followed by functionalization with hyaluronic acid PCN@MnO_2@DOX@HA. Hyaluronic acid helped in binding with CD44 receptors overexpressed on tumor cells, while in the presence of GSH, DOX was released and MnO_2 generated Mn^{2+} which could be used as T_1 MRI contrast agents. Furthermore, MnO_2 could catalyze the conversion of H_2O_2 present in cells to O_2 resulting in the reduction of tumor hypoxia, which in turn could be helpful for increasing the efficiency of cancer therapy.[93] Similarly, to address the issue of reactive oxygen species affecting the efficiency of radio-chemotherapy, and to achieve combined therapeutics delivery and MRI imaging, Zhao et al. reported flower-like MnO_2 nanoparticles modified with hyaluronic acid.[93] The particles were further loaded with H_2PtCl_6, which acts as an inhibitor for tumor cell proliferation. The efficiency of H_2PtCl_6 loading was enhanced here due to the presence of hyaluronic acid. The developed system also acted as a radiosensitizer, thus providing the possibility of combining radiotherapy with imaging and therapeutics delivery.[93] It is to be noted here that although MnO_2 nanomaterials-based contrast agents have been frequently explored in the literature, very limited studies have been performed so far by using them in combination of natural polymers providing a less explored platform for new theranostics.

In summary, various theranostic systems with tunable properties have been developed in recent years using different polysaccharides such as dextran, pullulan, gelatin, starch, cellulose, heparin, and hyaluronic acid. Table 2 provides an overview of recent examples of polysaccharides based theranostic systems that have been reported in the literature for combined drug delivery and MRI.

3.2. Theranostic Systems with CT Imaging Feature. In recent years, extensive efforts have been made to develop novel contrast agents for CT imaging that help in getting better contrast between the adjacent tissues, thus helping in better diagnosis.[113] In this regard, gold NPs have come up as an ideal candidate owing to the higher density and higher atomic number of gold.[114] To enhance the stability of gold NPs, their surface is modified with biocompatible small molecules or macromolecules. Although the surface modification of gold NPs with polyethylene glycol (PEG) improves their stability, the particles are not stable in the presence of GSH and high salt concentration.[115] Additionally, the coating with PEG hinders the cellular uptake of the developed modified NPs.[116] To address these issues, Sun et al. fabricated glycol chitosan (GC) modified gold NPs (GC-AuNP) showing stability and remarkable cancer targeting features owing to the presence of GC. The particles were also conjugated with peptides which could be activated by matrix metalloproteinase (MMP). The developed MMP-GC-AuNP provided the possibility of having optical imaging in combination with CT imaging (Figure 5).[117] It is to be noted here that having the targeting feature in a CT probe is extremely beneficial, and the use of different polysaccharides plays an important role in it. Hence, to further understand the importance of surface modification using GC,

https://doi.org/10.1021/acsbiomaterials.1c01631
ACS Biomater. Sci. Eng. 2022, 8, 2281−2306

Table 2. Overview of Recent Examples of Polysaccharide-Based Theranostics

sample	polysaccharides	contrast agent	therapeutics	imaging	remarks	ref
1	Chitosan	Fe_3O_4 NPs	Nanoceria	T_2 MRI	Electrostatic self-assembly and ionic gelation approaches; self-assembly based theranostics less cytotoxic as compared to ionic gelation; ROS scavenging capability	Wu et al.[94]
2	Chitosan	Gd^{3+}	Chlorin e6	T_1 MRI	Chitosan conjugated with octadecanoic acid and gadopentetic acid; self-assembly approach, negligible hemolysis and satisfactory ROS generation	Zhao et al.[95]
3	Chitosan	Fe_3O_4 NPs (MRI); Au NPs (CT)	Methotrexate	T_1 MRI	Surface coating with modified chitosan; good cytocompatibility; magnetic property and X-ray attenuation	Hemalatha et al.[96]
4	Metal organic framework@-chitosan	MIL-100 (Fe-BTC); Carbon dots	Doxorubicin	Dual T_2 MRI and optical imaging	Coating with *O*-carboxymethyl chitosan for improved biocompatibility and pH responsive drug release	Lin et al.[92]
5	Sodium alginate	Prohance [Gd(HPDO3A)(H_2O)]; Holmium ions	Fluorescein	T_1 MRI; T_2 MRI	Cross-linking by holmium metal ions, temperature responsive drug release	van Elk et al.[90]
6	Sodium alginate	Fe_3O_4 NPs	Paclitaxel	T_2 MRI	Coating with thiolated sodium alginate grafted with amine-terminated poly(butyl methacrylate); enhanced dispersion stability and drug encapsulation efficiency	Arora et al.[89]
7	Sodium alginate	Gd^{3+}	Rhodamine b	T_1 MRI	Alginate nanogel by reverse microemulsion and physical cross-linking; enhanced stability; presence of alginate reduces the T_1 relaxation time	Podgórna et al.[85]
8	Disulfide modified alginate	Fe_3O_4 NPs	Doxorubicin	T_2 MRI	Covalent binding of Fe_3O_4 NPs with disulfide modified alginate; pH and reducing environment responsive drug release; lower side effects to healthy cells	Peng et al.[66]
9	Gelatin	Silica coated Fe_3O_4 NPs	Paclitaxel and taxol	T_2 MRI	Coating with gelatin oleic acid; enhanced circulation time and regulated transportation of paclitaxel to tissues	Tran et al.[97]
10	Hyaluronic acid	Fe_3O_4 NPs	Homocamptothecin	T_2 MRI	Covalent conjugation of hyaluronic acid; accumulation in tumor tissue under the magnetic field; enhanced biocompatibility	Wang et al.[98]
11	Alginate, chitosan	Fe_3O_4 NPs, Au NPs	Gene delivery	Dual MRI and CT imaging	Assembly of alginate/chitosan polyelectrolyte in multilayer on metal NPs; enhanced stability and biocompatibility; pH responsive drug release; enhanced cell apoptosis	Yang et al.[99]
12	Catechol-grafted chitosan alginate	Barium sulfate microcapsule	Ranitidine hydrochloride	CT imaging	Self-assembly of catechol grafted chitosan on microcapsules; enhanced retention in stomach	Du et al.[100]
13	Glycol chitosan	Iodine-containing diatrizoic acid, perfluoropentane	-	Dual CT and ultrasound imaging	Chemical conjugation of iodine to glycol chitosan; physical encapsulation of perfluoropentane by emulsification	Choi et al.[101]
14	Chitosan	Au nanocluster	MMP-9 Plasmid shRNA	CT imaging	Azide−alkyne cyclization reaction for preparing chitosan-*graft*-poly(L-lysine); surface coating of modified chitosan; enhanced CT signal in comparison to commercial iohexol; enhanced plasmid delivery	Yu et al.[102]
15	Chitosan	Au nanorattle	Doxorubicin; photothermal therapy	SERS based imaging	NIR-responsive drug delivery, ROS generation; induces membrane blebbing	Sarkar et al.[103]
16	Chitosan/hollow mesoporous silica nanoparticles	CuS nanodots	Doxorubicin; photothermal therapy	Thermal/photoacoustic dual-modality imaging	NIR and reducing environment responsive drug release	Niu et al.[104]
17	Hyaluronic acid	WS_2 nanodots, Ce6	Photothermal, radiation, photodynamic combination therapy	Multimodal CT, Fluorescence, photoacoustic imaging	Hyaluronic acid/polyaniline hybrid shell on nanodots; enhanced tumor uptake; higher efficiency for radiation and photodynamic therapy	Wang et al.[105]
18	Hyaluronic acid	Molybdenum oxide NPs	Photothermal therapy	CT imaging	Improved precision of phototherapy by combination of CD44 receptor targeting and tumor microenvironment related pH responsiveness	Wang et al.[106]
19	Dextran	Iodine	Doxorubicin	CT imaging	Hydrogel microspheres *via* inverse suspension polymerization method; potential interventional embolization	Zhu et al.[107]
20	Dextran	Porous silicon; Au NPs	XMU-MP-1	CT imaging	Microfluidic method enables the incorporation of multiple NPs together in a single step; identification of pathological changes in liver tissue; improved drug solubility and drug functioning time as compared to free drug	Liu et al.[108]
21	β-Cyclodextrin-based poly(ε-caprolactone)-dextran star polymer	Fe_3O_4 NPs	Doxorubicin	T_2 MRI	Reducing environment responsive drug delivery; folate receptor mediated endocytosis	Yang et al.[109]
22	Chitosan	Fe_3O_4 NPs	-	T_2 MRI	8-fold increase in transverse relaxivity rate (r_2) reaching a maximum of 533 Fe mM^{-1} s^{-1}	Lin et al.[110]
23	Chitosan	Au NPs	Photothermal therapy	Photoacoustic imaging	Synergistic gene/photothermal therapy for breast cancer	Dai et al.[111]
24	Dextran or pullulan	Au nanorods	-	Photothermal therapy	Capability of responsive self-destruction	Song et al.[112]

https://doi.org/10.1021/acsbiomaterials.1c01631
ACS Biomater. Sci. Eng. 2022, 8, 2281−2306

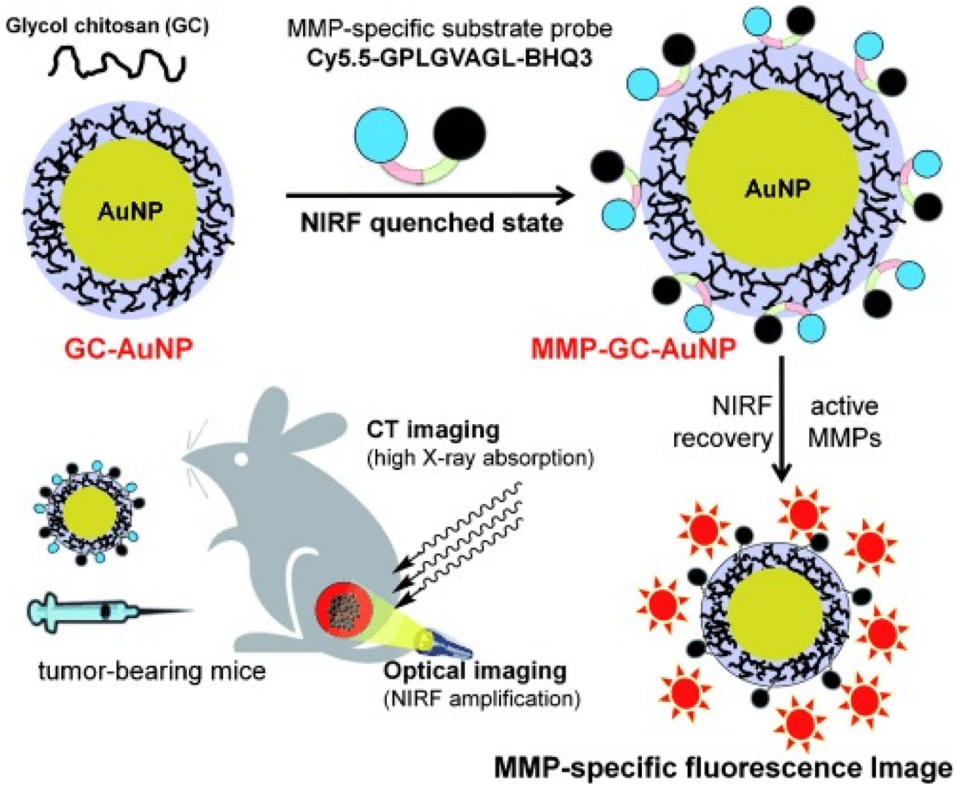

Figure 5. Schematic representation of MMP-GC-AuNP multimodal contrast agent for CT imaging combined with optical imaging. Reproduced with permission from ref 117. Copyright 2011 Wiley-VCH Verlag GmbH & Co. KGaA, Weinheim.

Sun et al. compared the tumor-targeting behavior of GC-AuNP and heparin-coated gold NPs.[118] It was reported that heparin-coated gold NPs were accumulated in normal tissue of the liver, while GC-AuNP targeted the tumor site.[118,119] Experimental results further indicated that accurate CT images could be obtained for liver cancer cells using GC-AuNP. Additionally, the presence of an amine group on the surface could also be explored for drug conjugation.[118]

Similarly, to develop an efficient CT-guided chemotherapy system, Keshavarz et al. synthesized alginate hydrogels loaded with gold NPs and cisplatin drug.[120] CT studies showed the increased CT contrast exhibited by the developed system. Cytotoxicity experiments exhibited higher tumor cell killing efficiency of gold NPs and cisplatin drug-loaded alginate hydrogels as compared to free drug. On the other hand, Li et al. synthesized gold-coated Fe_3O_4 nanostars stabilized by hyaluronic acid, which could be successfully used for dual CT and MR imaging *in vivo*.[121]

Further, cellular uptake of the nanoparticles is not only influenced by their size but also by their shape. It has been reported that the particles having higher aspect ratio can be internalized more readily than spherical ones.[122] Hence, to explore the potential of nonspherical contrast agents in multifunctional therapy, Hu et al. used spindle-shaped cellulose nanocrystals which were modified with synthetic polymer-based heterogeneous polymer brushes.[123] The surface-modified cellulose nanocrystals were further used as a template for *in situ* growth of gold NPs. The developed system was successfully used for CT imaging and gene therapy displaying its capability for multiple actions in treatment.

In another direction, research attempts have also been made to develop the CT contrast agent via a green chemistry method for targeted imaging. In this regard, Uthaman et al. synthesized mannan-functionalized gold NPs (M-GNPs) by using mannan as both a reducing and stabilizing agent (Figure 6a).[124] Mannan is a bioactive polysaccharide which helped here in avoiding the use of external reducing agents such as $NaBH_4$. The overall synthesis was based on a green approach without involving any harmful chemical or solvent. The developed M-GNPs could target the lymph nodes and were effectively taken up by endocytosis with the help of mannan receptors expressed on the surface of cells (Figure 6b). M-GNPs were efficient as a CT imaging probe with maximum Hounsfield units of 303. The increasing accumulation of M-GNPs in lymph nodes as a function of time was also investigated with the help of silver-eosin staining (Figure 6c). It was reported that M-GNPs are selectively taken up by the macrophages and dendritic cells due to the presence of mannan receptors. In this way, the developed M-GNPs showed their potential for selective lymph node targeted CT imaging which is an active area of research.[124]

In their quest to explore other inorganic NP-based CT contrast agents, Du et al. prepared hyaluronic acid-coated Bi_2O_3 NPs for CT imaging.[125] Due to the presence of hyaluronic acid, the developed NPs were very stable and able to bind effectively to CD44 receptors overexpressed on the cancer cells. Hyaluronic acid-coated Bi_2O_3 NPs showed multiple activities by exhibiting efficient attenuation of X-rays along with providing radiosensitization causing cell apoptosis. In this way, the developed system could be a potential candidate for CT imaging guided radiotherapy of tumors due to the low cost of bismuth element as compared to gold and higher radiosensitization.[125,126] Similarly, other bismuth-based nanoparticles (such as Bi_2S_3 NPs and Bi_2Se_3 nanoplates) and

https://doi.org/10.1021/acsbiomaterials.1c01631
ACS Biomater. Sci. Eng. 2022, 8, 2281−2306

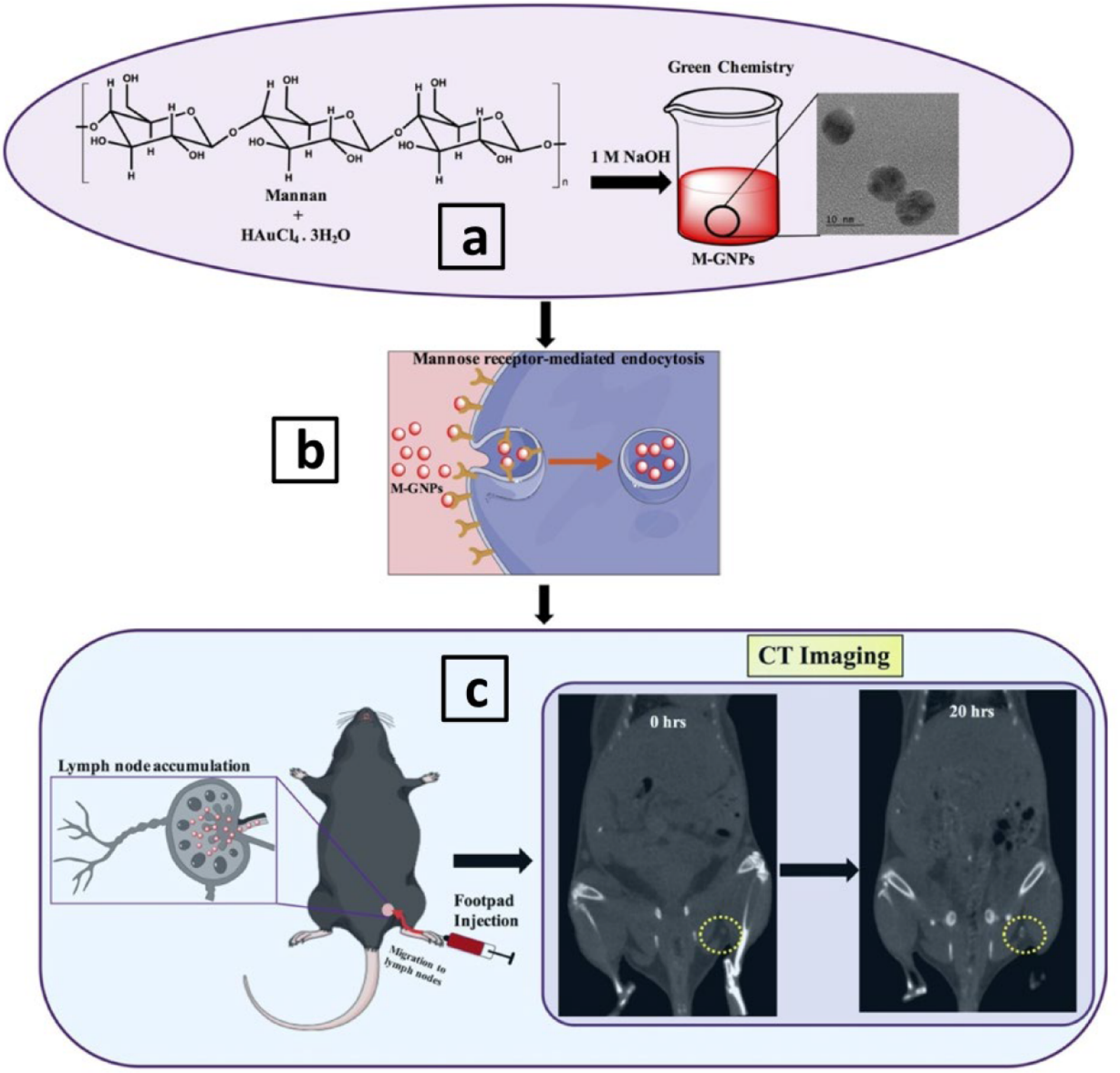

Figure 6. Scheme showing fabrication of M-GNPs as contrast agent for CT imaging (a); cellular uptake of M-GNPs via endocytosis (b); M-GNPs as CT imaging probe (c). Reproduced with permission from ref 124. Copyright 2017 Elsevier Ltd.

tungsten trioxide NPs are also able to attenuate X-rays with high efficiency.[127−129] However, few studies have reported the application of theranostics by combining polysaccharides with bismuth and tungsten-based nanoparticles.[125,130−134] due to the lack of functional groups for post-modification and difficulty in controlling their shape and size.

Apart from inorganic nanoparticles providing CT contrast, iodine-based low-molecular-weight molecules have also been used for CT imaging. As iodinated molecules are non-target-specific and exhibit lower retention time, it is difficult to obtain high-contrast images in short imaging time.[124,135] Hence, these small molecules have been used in combination with functional polymers to obtain desirable pharmacokinetics and target specific high contrast images. In this regard, Zhu et al. prepared iodixanol (Visipaque) containing hyaluronic acid nanogels (HAI-NGs) for breast cancer-targeted CT imaging and chemotherapy.[136] Herein, HAI-NGs were prepared by click reaction-based photo-cross-linking of the disulfide linkage containing polyiodixanol-methacrylate and hyaluronic acid-cystamine-tetrazole (Figure 7a). Further, paclitaxel anticancer drug was loaded in the developed nanogels for efficient chemotherapy. This paclitaxel-loaded HAI-NGs exhibited remarkable targeting ability for CD44 receptors and could degrade under the reducing conditions of cancer cells (Figure 7b,c). The circulation time of the contrast agent was effectively increased as compared to free iodinated molecules, thus presenting itself as a novel theranostic system for imaging guided therapy.[136]

Similarly, Lee et al. synthesized 2,3,5-triiodobenzoic acid-conjugated hyaluronic acid which self-assembled into multi-functional nanoparticles.[137] These NPs were loaded with doxorubicin as a model anticancer drug. Once again, the interaction between hyaluronic acid and CD 44 receptor was exploited here to ensure the uptake of developed nanoparticles by cancer cells. High-contrast CT images could be obtained in a SCC7 tumor-xenografted mouse model due to the presence of iodinated components in the NPs. Further, fluorescent dye Cy5.5 was also attached to the system to allow the possibility

https://doi.org/10.1021/acsbiomaterials.1c01631
ACS Biomater. Sci. Eng. 2022, 8, 2281−2306

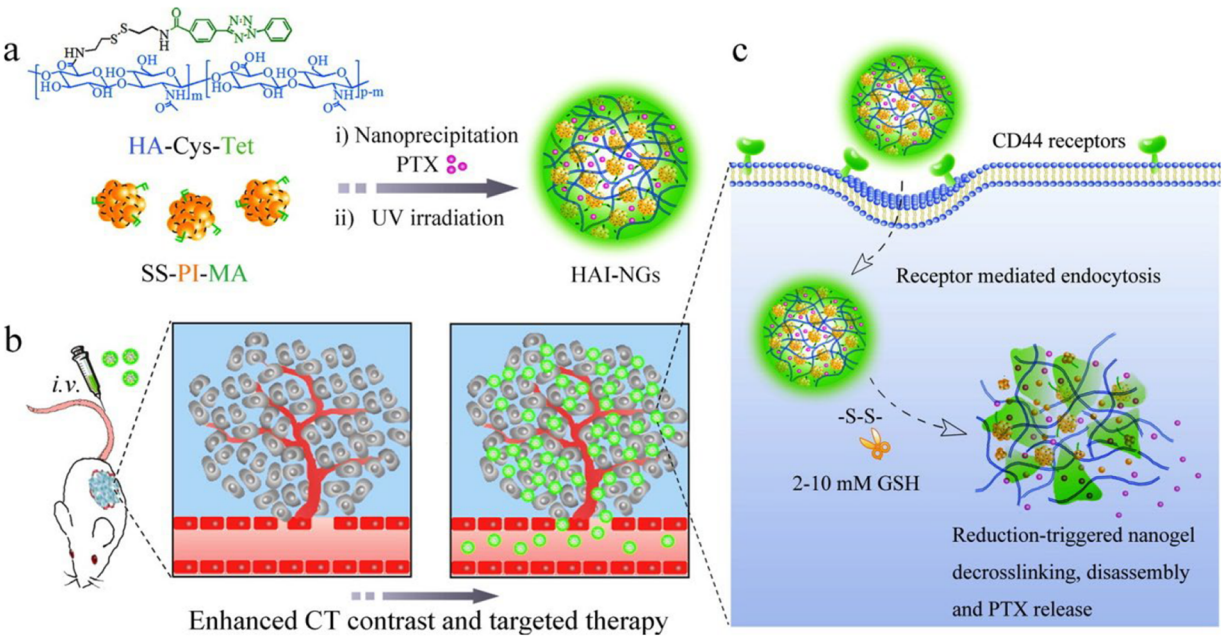

Figure 7. Preparation of paclitaxel (PTX) loaded HAI-NGs (a); schematic showing the accumulation of PTX loaded HAI-NGs in breast cancer cells (b); cellular uptake of PTX loaded HAI-NGs and their degradation in the presence of GSH (c). Reproduced with permission from ref 136. Copyright 2016 Elsevier Ltd.

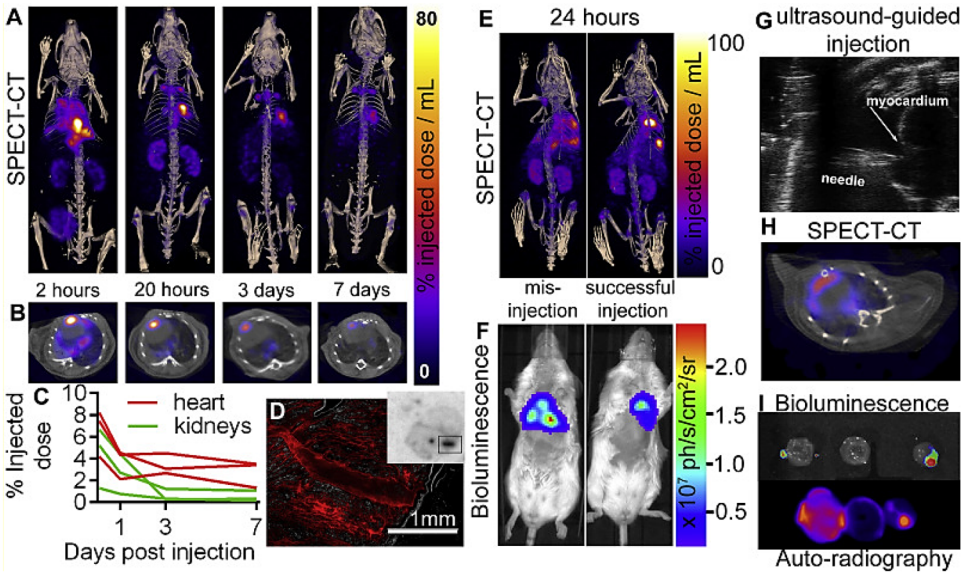

Figure 8. A. SPECT image showing retention of cardiac ^{111}In alginate implantation and excretion of nonretained material via the kidneys and bladder. B. Axial SPECT-CT sections show myocardial ^{111}In alginate colocalization. C. SPECT-CT ROI activity quantification shows longitudinal kinetics of ^{111}In alginate cardiac retention and excretion via the kidneys. D. Fluorescence microscopy of 20 μm sectioned heart tissue 10 days post-injection showing the TRITC-alginate injection tract, with the corresponding injection tract visible on the autoradiography image of the whole section. E. SPECT-CT of ^{111}In alginate + MSCs at 24 h following successful and unsuccessful injection, together with corresponding F. Bioluminescence images from the same mice confirm the location of live cells. G. Ultrasound-guided myocardial injection of ^{111}In alginate. H. Axial SPECT-CT section showing colocalization of ^{111}In alginate-MSCs SPECT signal with CT heart. I. *Ex vivo* bioluminescence showing live MSCs colocalized with ^{111}In alginate ^{111}In alginate at sites of implantation in corresponding *ex vivo* autoradiography of apical, mid, and basal heart tissue sections. Reproduced with permission from ref 150. Copyright 2020 Elsevier Ltd.

of near-infrared (NIR) fluorescence imaging, thus achieving multimodal imaging and chemotherapy.[137]

To investigate CT contrast alternatives apart from iodine-based molecules, Liang et al. synthesized multifunctional NPs using hyaluronic acid conjugated with two NIR dyes (Cy5.5 and IR825).[138] These NPs were loaded with perfluorooctyl bromide (PFOB), which in turn acted as CT contrast agent. Here, Cy5.5 provided fluorescent imaging, while IR825 provided the opportunity for photoacoustic imaging. Thus, the developed hyaluronic acid-based theranostic NPs showed multimodal imaging action for effective diagnosis. Various recent examples of theranostics systems, including a CT imaging feature, prepared by using a polysaccharide-based polymer matrix have been summarized in Table 1.

https://doi.org/10.1021/acsbiomaterials.1c01631
ACS Biomater. Sci. Eng. 2022, 8, 2281−2306

3.3. Theranostic Systems with PET/SPECT Imaging Feature. Early and precise diagnosis of cancer information is vital to construct the optimal treatment plan. Significant efforts are being made for advancement in fluorescent and radionuclide-based diagnostic tools which are helpful in cancer diagnosis.[139] In comparison to fluorescence imaging, nuclear/radionuclide imaging provides precise information with infinite penetration depth and also offers quantitative capability.[140,141] Of late, natural polymer-based complexes (nanoparticles and nanocrystals) and hydrogels tagged with radionucleotides have shown remarkable potential in SPECT/PET based imaging (Figure 8).[142,143] Metal-chelating properties of natural polymers have been explored by many researchers in cross-linking biopolymer-based hydrogels with radiometal cations to support noninvasive tumor imaging with SPECT/PET.[144−146] In order to design imaging probes for clinical applications, facile synthetic routes, uniformity, reproducibility, capability for scaleup, biosafety, and colloidal stability are some key aspects which need to be addressed.

Alginate is an important class of natural polymers and has been extensively explored for its role in various biomedical applications. Ca^{2+} cross-linked alginate hydrogels have been widely used to mimic soft tissues.[147−149] However, these hydrogels have also been associated with limitations of being detected by various imaging platforms like MRI, SPECT, and PET. To address these shortcomings, Patrick et al. tested the capability of $InCl_3$ and $ZrCl_4$ in cross-linking alginate to aid imaging of ^{111}In and ^{89}Zr with the help of SPECT and PET, respectively (Figure 8).[150] The work targeted 3D noninvasive nuclear imaging platform with good resolution across the anatomy and can be used for both preclinical and clinical trials. This system offered the possibility to image the whole body at the *in vivo* level by analyzing the retention and clearance of alginate-based hydrogels used in drug delivery via nasal and oral routes of administration. The work also demonstrated the colocalization of ^{111}In-alginate with mesenchymal stem cells (MSCs) at the site of implantation with in-depth biodistribution. This study emphasized the repeatability and long-term stability of the designed system as a key aspect to attain effective theranostic applications.

Further, Gholipour et al. developed a ^{68}Ga-dextran complex (GaD) for dual-modality PET/MRI imaging. The efficacy of the designed complex was tested under both acidic and alkaline conditions. The *in vivo* biodistribution of the fabricated GaD complex displayed its enhanced accumulation in the lungs with a substantial uptake that was detected in the cartilage tissues as well.[151] On the other hand, Keliher et al. developed a zirconium-89 (^{89}Zr) cross-linked short-chain dextran nanoparticle for a macrophage-specific PET imaging agent. With a half-life of 3.9 h, the designed system was found to be mainly located in tissue-resident macrophages when compared to other WBCs.[152] These strategies offered reproducibility, colloidal stability, and biosafety along with versatility to be used for various imaging platforms.

The microenvironment around a tumor is very difficult to categorize, and in order to gain a significant understanding regarding its structure and developmental mechanism, nanoparticles have played an important role.[153] Nanoparticles of varied shape and size are ideal candidates to combine drug delivery with imaging techniques such as PET/SPECT for proficient cancer therapy.[154,155] In a study, Imlimthan et al. developed Lutetium-177 (^{177}Lu)-labeled cellulose (LuC) nanocrystals loaded with vemurafenib as a multifunctional platform for drug delivery and noninvasive diagnosis of melanoma using SPECT imaging. LuC nanocrystals were investigated for their immunological behavior in murine and human melanoma cells. The efficacy of LuC nanocrystals was also analyzed in a mouse model bearing melanoma allografts in the lung. The LuC nanocrystals offered complementary radiolabel stability, better drug release profile, cellular uptake, and inhibition of cell growth at the *in vitro* level. The biodistribution of LuC nanocrystals *in vivo* revealed substantial retention of the LuC nanocrystals in the lung, liver, and spleen.[156] The results obtained for LuC nanocrystal-based SPECT imaging could have a fascinating future in potential clinical applications.

Researchers have developed and utilized a variety of polymer-based platforms for multimodal imaging applications. Consistent efforts to develop even more sophisticated polymer-based imaging probes have been the driving force for many research groups. The versatility of chitosan has identified it as a potential biopolymer in many theranostic applications.[157,158] Hwang et al. developed ^{131}I-labeled chitosan hydrogels for theranostic applications for liver cancer. SPECT was utilized to study the tumor induction rate, which was reported to be around 72% with major accumulation of ^{131}I-labeled chitosan observed in the liver.[159] The system offered negligible extrahepatic deposition and provided evidence for a new class of radioembolization devices with substantial therapeutic potential for MR/SPECT-based imaging applications. In another study, Pang et al. developed a chitosan−collagen-based composite microsphere (CCM) and radiolabeled it with Iodine-131 (^{131}I) for hepatocellular carcinoma (HCC) treatment. With a high processed efficiency of 70.4 MBq mg^{-1} of microspheres, the system also offered colloidal stability at the *in vitro* level. The designed system could be used for dual-imaging applications with regression in tumor size as indicated through SPECT/MR imaging. Adequate localized biodistribution upon administration along with steady stability of ^{131}I-CCMs in the liver over a period of 28 days showed the competence of ^{131}I-CCMs as a probable candidate for cancer theranostics.[160]

On similar grounds, Lee at al. radiotagged ^{64}Cu to chitosan (CuC) nanoparticles through click chemistry via a strain-promoted azide−alkyne cycloaddition strategy with a high radiolabeling efficiency and yield of almost 98%. Adequate colloidal stability and negligible effect on the physicochemical properties (zeta potential, spherical morphology) of chitosan were added advantages associated with the designed system. Upon intravenous administration of CuC nanoparticles in tumor-bearing mice, tumor targetability and real-time *in vivo* biodistribution were analyzed with the help of micro PET.[161] Facile synthetic route and higher yield marked the potential of this system as a potent tool for PET-based tumor imaging.

To impart multimodal imaging ability, thereby enhancing the versatility of chitosan, Lee et al. fabricated a dual-mode imaging probe for PET/optical imaging based on glycol chitosan nanoparticles (CNPs). To fabricate the dual PET/optical probe based on CNPs, both ^{64}Cu-radiolabeled DOTA complex and activable matrix metalloproteinase (MMP)-sensitive peptide were tagged onto CNPs with the help of bio-orthogonal click chemistry through chemically reacting azide group and dibenzyl cyclooctyne.[162] *In vivo* biodistribution and the expression of MMP-sensitive peptides were monitored in tumor-bearing mice with the help of PET/optical imaging. Further, Polyak et al. manufactured poly(γ-glutamic

https://doi.org/10.1021/acsbiomaterials.1c01631
ACS Biomater. Sci. Eng. 2022, 8, 2281−2306

acid)/folic acid/chitosan-based self-assembled nanoparticles with high colloidal stability and radiolabeled them with technetium-99m (^{99m}Tc). The system was studied for its potential as an effective SPECT/CT imaging agent in order to diagnose tumors with augmented levels of folate receptors. The results concluded that there was enhanced activity along with slow elimination from the heart, liver, kidneys, and urinary tract.[163] Extensively higher uptake (9% of administered dose) was recorded for the HeDe (Hepatocarcinoma Debreceniensis) tumor cell line transplanted Fischer 344 rat models compared to 2% in control rat models. The study suggested the potential of using the fabricated system for clinical translation. Collectively, the studies revealed the fact that in order to design an effective and efficient PET/SPECT agent, the imaging time frame after dose administration plays a key role. This factor could be applied for further investigation in order to amend the existing polymer-based systems in order to develop more sophisticated and efficient imaging-based clinical applications.

To investigate the folate receptor-targeted radionucleotide-tagged agent for multimodal imaging for detecting ovarian cancer cells, Korhegyi et al. developed modified folic acid nanoparticles and conjugated them with chitosan-modified chelator (NODAGA-NHS) followed by radiolabeling with Gallium-68 (^{68}Ga) (III) ions. PET/MR dual imaging showed enhanced tumor uptake with a 6.5 tumor-to-muscle ratio.[164] Selective binding of the designed nanoparticles was observed at an *in vitro* level in folate receptor-positive (KB) and negative (MDA-MB-231) cell lines. Subcutaneous administration on tumor-bearing CB17 SCID mice models provided significant uptake of the nanoparticles at an *in vivo* level as studied by PET/MR dual imaging. These examples clearly indicate the potential of chitosan in the development of radionucleotide-tagged systems for SPECT/PET imaging.

The cited examples and studies given above shows the importance of chitosan in development of imaging probes for SPECT/PET imaging. Further, natural polymers like dextran, hyaluronic acid, and heparin have significant target abilities and because of less complexity and low molecular weight could easily be maneuvered and controlled for theranostic applications. This could provide room for further investigation in an attempt to develop more potent, stable, and longer-lasting imaging probes for SPECT/PET imaging.

3.4. Theranostic Systems with Ultrasound Imaging Feature. Ultrasound (US) is one of the most commonly used methods in diagnosis and disease therapy. Deep tissue penetration efficiency, safety, and noninvasive character are key aspects that mark the success of US in the medical field.[165,166] US has emerged as a potent candidate in the delivery of diverse therapeutic agents (Figure 9). US aids in delivering the payload at the right time in the right place.[167] The capacity of combined ultrasound imaging and synergistic chemoradiotherapy (CRT) was studied by Shang et al., who designed pH- and US-responsive perfluoropentane-encapsulated paclitaxel (PTX)-loaded carboxymethyl chitosan nanodroplets (NDs) by a homogenization/emulsion method. NDs presented enhanced proficiency in pH-dependent charge conversion, biocompatibility, and ultrasound contrast echogenicity.[168] The results obtained through biochemical assays (CCK-8 assay; migration assay) and flow cytometry presented enhanced cell response in CRT for PTX-loaded NDs. Further, Zhiyi and co-workers designed DOX-loaded carboxymethyl-hexanoyl chitosan (CHC) NDs with a core of perfluoropentane (PFP) using an oil in water (O/W) emulsion method.[169] An *in vitro* model was established to further evaluate the ultrasound imaging application of CHC-PFP-DOX NDs under different parameters. The antitumor effect of US combined with CHC-PFP-DOX NDs on ovarian cancer cells was also investigated. Ultrasound behaves as an external stimulus to enhance the drug releasing behavior as well as the cancer killing efficacy of the system. Though the designed system offered significant results at the *in vitro* level, the real-time functioning and biodistribution of any designed system under consideration could be adequately analyzed only after *in vivo* studies. In line with this, Baghbani et al. developed ultrasonic responsive alginate-stabilized perfluorohexane NDs with a size of around 100 nm for breast cancer therapy. DOX was loaded in the synthesized system and was evaluated for antitumor activity at *in vitro* and *in vivo* levels. Under the action of ultrasound triggering of drug release, the enhanced imaging capacity of the designed nanodroplets was confirmed.[170] These studies hold great promise in delivering ultrasound-mediated cancer-targeting imaging along with delivery for cancer therapeutics.

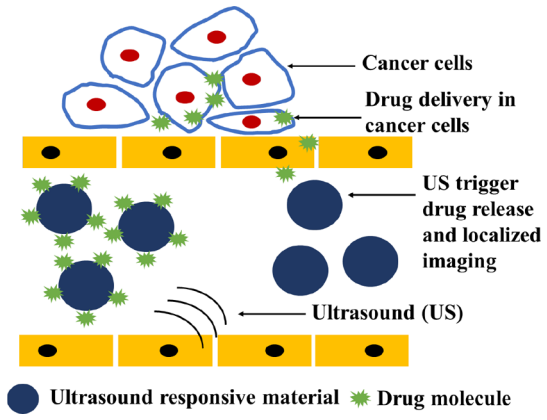

Figure 9. Ultrasound-triggered drug release and localized imaging.

Ultrasound-targeted delivery of nanobubbles (NBs) has also been credited as a promising approach for noninvasive drug delivery mechanism. Upon reduction of the size of US contrast agents, the intensity of the ultrasound echogenic signals decreases, which in turn reduces the stability of the bubbles. Consequently, designing NBs of size less than 200 nm with good imaging proficiencies and enhanced stability for long-term imaging *in vivo* has been the requirement to address the necessities of a designed system being marked as an efficient system for theranostic applications. To address this challenge, Zhou et al. designed a core−shell structure of approximately 120 nm in size with PFP as the core and chitosan as the shell of the NBs. DOX was loaded inside the NBs, and the system was studied for its drug delivery capacity. A clinical ultrasound imaging system was used to assess the capability of chitosan-based NBs for ultrasound triggered drug release and image enhancement. The anticancer effect of the designed chitosan-based NBs was evaluated following ultrasound-targeted nano/microbubble destruction (UTN/MD).[171] Similar study was carried out by Yu and co-workers who designed PFP-filled chitosan poly(acrylic acid) (PFP-CS-PAA) NBs with a size of around 100 nm via a direct core-template-free strategy. The prepared PFP-CS-PAA NBs were reported to exhibit imaging capabilities in nude mouse tumors for 7 days, post-administration.[172] These studies indicated the importance of

https://doi.org/10.1021/acsbiomaterials.1c01631
ACS Biomater. Sci. Eng. 2022, 8, 2281−2306

long-term stability of the designed material along with parameters that could be modulated for enhanced imaging time frame at *in vivo* levels.

Natural polymer-based hydrogels have also been used for ultrasound-triggered drug release. Huebsch et al. fabricated an alginate-based cross-linked hydrogel having the capacity to present US-triggered drug release along with self-healing properties.[173] These hydrogels were prepared by cross-linking alginate cross with Ca^{2+}. The study revealed negligible damage to the structure of hydrogels upon exposure to US but enhanced the drug release profile. The findings may provide vital insights in the area of US-responsive hydrogels. Working on a similar strategy, Husseini and his research group targeted the overexpressed hyaluronic acid (HA) receptor on the surface of breast cancer.[174] They successfully synthesized PEGylated liposomes encapsulating the anticancer drug calcein and conjugated it to HA. Upon expose to low-frequency ultrasound, significant enhancement of calcein uptake was observed for breast cancer cells compared to the nonexposed cells. The studies emphasize the importance of ultrasound as an external stimulus with its application in instant switch-on and -off release of therapeutic molecule loaded in a carrier.

To achieve an effective theranostic platform for cancer treatment, multifunctionality in research should be implemented. The ultrasound-triggered drug release could be combined with growth factors or healing properties of the base material used. This will not only aid in the treatment and imaging process but also supplement the fast recovery and growth of healthy cells. Widespread experimental efforts should be made in the direction of designing ultrasound-triggered natural polymers like dextran, heparin, and so forth, which are under less consideration. This will help in widening the horizon of natural polymer-based theranostic platforms and could also be helpful in further understanding the interaction of these natural polymers at cellular and *in vivo* levels.

To further improve the treatment efficacy and diagnostic ability of theranostic agents, one has to be very cautious to check the incompatibilities between the medications that are to be administered and the imaging contrast agents of choice. There have been reports and clinical instances where water-soluble contrast media have shown incompatibility with a range of pharmacological agents including some vasodilators, antihistamines, and even antibiotics.[175,176] Further, Zagoria et al. reported potential chemical incompatibility of low-osmolality contrast agents (hexabrix) with vasodilators (papverine, tolazoline) used in angiography.[177] It was observed that a mixture of hexabrix and papaverine produced a white precipitate, whereas hexabrix and tolazoline demonstrated temporary immiscibility. In the field of radiology, contrast agents and medications are frequently infused with indwelling intravenous lines. Incongruity between the contrast media and therapeutic molecules could result in precipitation which may have severe consequences like obstruction of the intravenous line, inactivation of the medication, and embolism.[178] Choice of contrast agent and drug is very important when designing theranostic systems, as incompatibility among them may lead to severe consequences including discomfort for the patient and fatality.

Further, a key challenge in designing polysaccharide-based theranostic systems is the adverse effects that are associated with polysaccharide functionalization. In addition, formulating a controllable and reproducible process with minimal batch to batch variation also restricts the commercialization of polysaccharide-based theranostics systems. The choice of polysaccharide also plays an important role in formulating an effective theranostics system. Pore size, molecular weight, cross-link density, and mechanical attributes are some key parameters that could decide the fate of the designed system at both pre- and post-administration level. For example, MRI contrast of Gd-based contrast agent can be enhanced with the help of conjugation with various polymers (e.g., polysaccharides), as it helps in increasing the molecular weight of the system, which in turn affects the tumbling rate.[79] Hence, in order to formulate an effective theranostic system, compatibility among the constituents along with the choice of application and targeted ailment has to be selected very wisely.

4. TOXICITY ASSESSMENT

Combination of therapeutic and imaging modalities in one probe, being a crucial feature of theranostic agents, may lead to contradicting expectations when applied *in vivo*. While a therapeutic agent aims at treatment of a disease with minimal impact to the healthy organs, an imaging agent is designed to visualize the pathology and be rapidly excreted from the body without any effects. Hence, the toxicity considerations must include both aspects and be approached carefully. As already mentioned, one of the strategies in designing theranostic agents is construction of nanomaterials. Therefore, in this section the potential toxicity assessment of polysaccharides along with each imaging modality will be reviewed first, followed by the discussion on general nanotoxicity.

4.1. Toxicity of Polysaccharides. In general, polysaccharides are nontoxic in nature, and many polysaccharides have been approved by the FDA for biomedical usage. However, there are studies which have reported the toxic effects of polysaccharides. Typically, chemical modifications and functionalization of polysaccharides have been associated with toxicity profiles. It is very interesting to note that the formulation strategies associated with polysaccharide-related probes alter the cellular uptake dynamics and affects their intrinsic safety profile. Studies conducted by Schipper et al. showed the toxic effects of chitosan of different molecular weight and degree of deacetylation (DD) on CaCo-2 cells, HT29-H, and *in situ* rat jejunum. Through this work, it was reported that higher DD in the case of high-molecular-weight chitosan imparts more toxic effects.[179,180] Further, trimethyl chitosan (quaternized chitosan) has been reported with very low cytotoxicity (IC_{50} > 10 mg/mL) for degrees of quaternization below 55%. However, Kean et al. reported the toxic effect of trimethyl chitosan with high degree of quaternization. This toxic effect was also reported in the case of higher-molecular-weight derivatives (100 kDa) of trimethyl chitosan.[181] The derivatization of chitosan needs further examination in order to comprehend the safety profile linked with it for their widespread applicability. In another study, Flexner et al. reported slight toxicity associated with dextran sulfate when administered continuously in subjects exposed to symptomatic HIV. Profound but reversible thrombocytopenia was reported in subjects receiving drug for more than 3 days and extensive but reversible alopecia in a few subjects.[182] Moreover, there have been few studies in which the anaphylactoid reaction of dextran has been reported in rats.[183−185] Further, Seo et al. reported the genetic toxicity (chromosomal damage) incurred by dextran-coated SPION in HepG2 cells by formation of intracellular ROS.[186] The study did not link dextran directly to the observed toxic effects, but

https://doi.org/10.1021/acsbiomaterials.1c01631
ACS Biomater. Sci. Eng. 2022, 8, 2281−2306

the nontoxic nature of dextran in this study needs further investigation. In another study, Sokolsky et al. reported the toxicity of oxidized dextran on AW 264.7 cell line with an IC_{50} of 3 μmol/mL aldehydes.[187] Although dextran is commercially used for many biomedical applications, analysis of the toxicity profile of their modified versions needs to be undertaken, for their utility at commercial levels. In order to investigate the toxicity profile of carboxymethyl cellulose (CMC), Baran et al. introduced CMC in the yolk sac of the zebrafish embryo.[188] CMC showed negligible toxicity but was associated with increased lipid accumulation in a dose-dependent manner. Recently, in a study conducted by Fan et al., adverse effects were reported in rats upon administration of high doses of sodium CMC (2000 mg/kg), while trivial reactions were reported upon administration of mild doses (320 mg/kg).[189]

Overall, polysaccharides are an integral part in designing healthcare tools which play an important role in many vital biomedical applications. Although not many toxicity issues have been linked with polysaccharides, new chemically modified derivatives of naturally occurring polysaccharides have been reported with certain adverse effects, if not severe. A detailed assessment of the safety profile of these derivatives will not only help to understand the in-depth cellular responses linked with their administration but also create a platform for their successful commercialization.

4.2. Toxicity of MRI Contrast Agents. The contrast agents used in clinics to enhance MR images are typically small paramagnetic complexes that have been considered safe when used at the recommended doses of 0.1−0.3 mmol of metal ion kg^{-1}. Currently, the main concerns are related to the use of Gd^{3+}, as this lanthanide (Ln) ion, like all members of the series, is extremely toxic when released in its free form. The structures of the ligands complexing Gd^{3+} can be classified as macrocyclic or linear, in which the metal ion is incorporated either in a preorganized cage or in an open-chain molecule, respectively. The charge of the complexes can be neutral, anionic, or cationic. Thereby, macrocyclic and ionic complexes are considered more stable based on their kinetic and thermodynamic stability constants. High kinetic stability indicates dissociation rate of Gd^{3+} ion from the complex being significantly slower than the elimination rate of the entire contrast agent from the body, while high thermodynamic stability refers to the high energy required to release the free Gd^{3+}. The presence of competing ions (Zn^{2+}, Ca^{2+}, Mg^{2+}, etc.) in the bloodstream can additionally challenge the overall stability of the administered contrast agent by induction of the transmetalation process. The toxicity mechanism in this case is based on the exchange of Gd^{3+} with the endogenous ions with the subsequent accumulation of the free ions in bones and skin.[190] Furthermore, Gd^{3+} can act as a substituent of Ca^{2+} and block voltage-gated channels and/or interfere with the function of metabolic enzymes.[191] Patients with normally functioning kidneys are able to eliminate >95% of the contrast agent within 24 h post-injection, while patients with renal dysfunction retain the complexes for a longer time during which dissociation of toxic Gd^{3+} can take place. The first indication of possible adverse effects by such patients was reported in 2006, when the use of Gd was associated with nephrogenic systemic fibrosis (NSF).[192] Ten years later, deposition of Gd in the brain was documented for the patients that underwent repeated MRI examinations with a linear Gd^{3+}-complex Omniscan (Gd-DTPA-BMA),[193] which was found to be 4-fold higher than for the cyclic contrast agent ProHance (Gd-HPDO3A).[194] The explanation can be found in the literature reporting transformation of Gd-DTPA and Gd-DTPA-BMA upon entrapment by fibroblasts and macrophages and the subsequent enzymatic reaction leading to N-oxidation of the acetic pendant-arm and release of free Gd^{3+}.[195]

In the search for alternative Gd-free contrast agents, much attention has been devoted to manganese (Mn), which is another paramagnetic metal with properties suitable for a sufficient positive contrast enhancement in MRI. In contrast with lanthanides, Mn is a systemic element that is part of the human diet and acts as a cofactor for metabolic enzymes and receptors. Despite demonstration of virtually no toxic effects in mice upon exposure to $MnCl_2$ for 3 weeks,[196] the complexation of Mn^{2+} by strong chelators is still required for the design of safe contrast agents. The main reason for this is the neurotoxicity of Mn caused by deposition of free ions in the brain known as "manganism", which is a neurodegenerative disorder resembling Parkinson's. Currently, one of the best candidates for the chelation of Mn^{2+} is a hexadentate ligand *N*-picolyl-*N*,*N*′,*N*′-trans-1,2-cyclohexenediaminetreacetate (Py-C3A) that provides stable binding while maintaining high relaxivity. The dissociation of free Mn^{2+} from this complex in the presence of an excess of Zn^{2+} was reported to be 20 times lower than that of Mn-DTPA.[197] Finally, Mn-nanoparticles become increasingly attractive due to literature data reporting good safety perspectives. However, the variety of Mn oxidation states (from −3 to +7) possibly coexisting during construction and especially application of nanoparticles should be considered, as some oxidation forms can enter redox reactions *in vivo* more easily than the others.[198]

The lack of long-term tolerance data on the Gd-free MRI contrast agents, which are currently under intensive scrutiny, clearly represents a challenge, and effective technologies for introducing these agents into theranostic systems are still to be developed. However, the extensive knowledge gained with conventional contrast media will not only facilitate this process but also help to clarify whether the use of the alternatives is justified. There are reports that suggest that Gd could stay in the body for months to years after being introduced during an MRI scan, leading to gadolinium retention (accumulation in liver, kidney, bone, and brain).[199,200] In order to understand cellular response to Gd and the pattern of removal, studies could be conducted using microfluidic-based 3D on chip models. The real-time information of these innovative devices could help in understanding many underlying mechanisms and further aid in developing new contrast-based strategies with acceptable safety concerns.

4.3. Toxicity of CT Contrast Agents. Iodinated small-molecular contrast agents are applied routinely in clinics to enhance contrast in CT scans. The initially proposed sodium iodine was abandoned shortly after due to its systemic toxicity.[201] The current CT contrast agents are typically mono- or dimeric derivatives of the benzene ring, where positions 2, 4, and 6 are substituted with iodine atoms, while other positions are functionalized with either ionic or nonionic groups. The binding of iodine to the benzene ring is stable, and the side chains make the molecules soluble in water; thus from this point of view, these contrast agents do not raise any toxicity concerns. However, the osmolarities and viscosities greater than those of the plasma or cerebrospinal fluid are known to cause mild adverse effects (e.g., itching and cutaneous reactions) as well as life-threatening emergencies (e.g., allergies or anaphylactic reactions).[202] Contrast-induced

https://doi.org/10.1021/acsbiomaterials.1c01631
ACS Biomater. Sci. Eng. 2022, 8, 2281−2306

nephropathy (CIN) is an acute kidney disease found to be one of the main problems associated with iodine-containing contrast media administered intra-arterially and, to a lesser extent, intravenously.[203] Thereby, the ionicity of the compounds and the accompanying osmolarity values seem to be playing an important role. Ionic agents (diatrizoate, metrizoate, ioxaglate) can be high-osmolar (HOCM) or low-osmolar (LOCM) with the osmolarities 8 to 2 times higher than that of plasma (300 mOsm/kg). With the advent of non-ionic LOCM (iopamidol, iohexol) and iso-osmolar (IOCM) contrast agents (iodixanol), most of the osmotoxicity issues could be resolved, which, however, did not eliminate concerns on general nerphrotoxicity related to tubular cells apoptosis, disruption of calcium homeostasis, and renal medullary ischemia, especially in renally impaired patients.[204]

Incorporation of iodine species into various polymeric structures was proposed as an attempt to solve the aforementioned toxicity issues.[205] However, with the longer blood circulation times of such nanosystems, the preference clearly goes to the formulations where the iodinated parts are excreted along with the carrier. It was demonstrated that during clearance of liposomes by the reticuloendothelial system, the released iodixanol accumulates in the liver where it undergoes biotransformation and results in adverse effects even at moderate amounts of this contrast agent (up to 100 mg I/kg).[206]

Novel CT contrast agents based on gold (Au) and bismuth (Bi) are currently gaining attention due to their physical properties in combination with low toxicity. For instance, hemolysis caused by a small Bi-DTPA complex was shown to be negligible at the concentrations up to 500 μM,[207] and even less toxicity was reported for the nanoparticulate formulations of Bi compared to its ionic form.[208] Generally, heavy metals are very attractive for the development of efficient CT agents, based on the higher X-ray attenuation and thus lower concentrations required for sufficient contrast compared to classic iodine-based CT agents.

4.4. Toxicity of PET/SPECT Imaging Agents. The evolution of radionuclide imaging shows a clear preference for diagnosis where the high sensitivity of PET/SPECT is combined with the high anatomic resolution of CT. The safety considerations for such hybrid systems mainly concern exposure of the patients to the harmful X-ray radiation originating from the CT-modality, which is reviewed extensively in the literature.[209] On the other hand, the tracers applied for both PET and SPECT imaging are less of a problem in terms of radiotoxicity, since they are generally short-lived radioisotopes that are excreted from the body by the renal system within 24 to 48 h after their intravenous administration. In this context, it is important to realize that the picomolar amounts of tracers administered for radionuclide imaging omit any chemotoxicity concerns, even if the elements involved are chemically toxic by nature. On the other hand, envisioning radionuclides for therapeutic purposes requires careful estimations of the radiation amount absorbed by the organs with the minimal off-target damage and the doses administered to the patients.[210]

Generally, the radiation dose to which a patient is exposed during PET and SPECT with conventional radiotracers ranges from 4 to 8 and 10 to 30 mSv, respectively. Advances in 3D imaging as well as extended-field-of-view and time-of-flight modalities typical for the new generation of PET-CT scanners allow for reduced doses of applied radiopharmaceuticals.[211] Moreover, low signal-to-noise ratio due to either unspecific distribution of the tracer or the large size of the patient can in some cases be circumvented by the increase of the image acquisition time without exposure to a higher dose.[212]

Enclosure of radioisotopes into essential biomolecules without changing their properties, thus sustaining metabolic processes, is a common way to perform radionuclide imaging. Illustrative examples are ^{18}FDG (^{18}F $t_{1/2}$ = 110 min) that is a gold standard used in PET for identification of abnormal glucose metabolism and ^{11}C-methionine (^{11}C $t_{1/2}$ = 20 min) applied for the PET imaging of various cancers. Importantly, the administered doses per patient in these cases correlate as 1000 times lower than the corresponding concentrations of stable analogues that are considered toxic.[213]

Even though the small amounts of radiopharmaceuticals can provide activities sufficient for acquisition of images, a stable chelation is required in the case of metallic tracers to ensure their safe clinical application. For example, complexation of a common PET radioisotope $^{68}Ga^{3+}$ by suitable small-molecular ligands (DOTA/NOTA) can prevent its binding to transferrin *in vivo* as the result of mimicking Fe^{3+}.[214] For some cations with a more complicated coordination core, such as a positron emitter $^{89}Zr^{4+}$ ($t_{1/2}$ = 78.4h), the classic coordination yields a complex whose stability is not sufficient to endure the long exposure to the *in vivo* environment. The small atomic radius of Zr in combination with the variable coordination number (4−9) requires polyanionic hard donors for a stable complex formation. One of the accepted routes for a stable ^{89}Zr-complexation is utilization of the desferrioxamine moiety,[215] which can additionally be applied in combination with various nanocarriers, e.g., dextran nanoparticles of 13 nm, that were demonstrated to be nontoxic in mice.[152] The same strategy is carried out for conjugation of ^{89}Zr with monoclonal antibodies for PET imaging preceding radioimmunotherapy with ^{90}Y. As excretion of these peptide-based probes goes through the kidneys, retention of radionuclides in the proximal tubules can potentially induce nephrotoxicity. A way around this problem was found in coadministration of negatively charged amino acids that competitively inhibit the binding of radiopeptides and reduce the radiation exposure of the kidneys.[216]

In conclusion, PET/SPECT radiopharmaceuticals administered in microdoses are not considered harmful as such. However, in theranostic formulations, longer retention/circulation times as well as possible repetition scans for response monitoring might cause adverse effects. Therefore, along with careful dose optimization, aspects such as pharmacokinetics, stability in the presence of enzymes, and metabolic pathways should be taken into account.

4.5. Nanotoxicity. Initially, nanotherapeutics were considered in the clinic due to their ability to improve the effects of their small-molecular counterparts by increasing the solubility of drugs and reducing the required therapeutic dose through more effective accumulation in diseased organs. This approach introduced concerns on nanotoxicity, which is assessed routinely by *in vitro* experiments evaluating the cytotoxicity. However, aspects such as biodistribution, accumulation, metabolism, and excretion of nanoparticles play an important role in their clinical acceptance.

Among general toxicity issues reported for various nanoparticles, the most important ones are related to their size, shape, and surface activity that can be displayed at molecular, cellular, and tissue levels. Examples of such effects are induction of mesothelioma caused by carbon nanotubes due

https://doi.org/10.1021/acsbiomaterials.1c01631
ACS Biomater. Sci. Eng. 2022, 8, 2281−2306

to their elongated shape,[217] size dependency of gold nanoparticles that are found to be toxic at a diameter of 1.4 nm compared to the nontoxic analogues of 15 nm diameter,[218] and generation of reactive oxygen species (ROS) by iron oxide nanoparticles.[219] An exception is microbubbles for ultrasound imaging that do not cause any toxicity concerns except for some rare and self-resolving allergic reactions.[220]

Further, the surface of nanoparticles is prone to interaction with biomolecules present in biological fluids, which may not only alter the properties of the probe but most importantly also induce unfolding of proteins such as albumin, cytochrome, and ribonuclease, which subsequently compromises their function. Such effects have been reported for intravenously injected iron oxide nanoparticles that were shown to change the structure of transferrin by causing an undesired release of iron and as a result affecting the *in vivo* iron transport.[221] Grafting of polymers to the surface of nanoparticles is a common way to bypass such undesired events and to prolong the blood circulation times of the nanoprobes to serve the theranostic purposes, but at the same time, it poses concerns related to hepatocellular toxicity.[222] The main problem in this case remains the possibility for a long-term dissociation of metal ions and possible toxicity of the coating molecules. Biological and biocompatible macromolecules such as polysaccharides, PEG, and poly(lactic acid) have been demonstrated to be superior in this respect due to their nontoxicity and tolerance to mammalian tissues,[223] provided sufficient coverage is applied.[224] However, attention should be paid to the methods used for conjugation of the biomolecules to the surface of nanoparticles or cross-linking of the biopolymers to construct theranostic systems. For example, application of an efficient linker glutaraldehyde was shown to limit cell viability.[187] Therefore, the preference should be given to biocompatible linkers, such as carbodiimide and succinic, malic, tartaric, and citric acids.[225] Additionally, the surface charges originating from the coating molecules determine the nanotoxicity. Hoskins et al. compared PEGylation of SPIONs with poly(ethyleneimine) (PEI) coating and demonstrated cytotoxicity of PEI-nanoparticles due to higher positive charges, and hence greater formation of ROS and lipid peroxidation.[226] The importance of an appropriate coating is furthermore clear from the examples of nanoparticles composed of biocompatible metals, such as gold. While cationic Au nanoparticles were demonstrated to induce oxidative DNA damage,[227] the lysine-coated analogues were found to be nontoxic at concentrations up to 100 M.[228]

Commonly, nanoparticles tend to exhibit less toxicity compared to their ionic equivalents; it was demonstrated that Au nanoparticles are ten times less toxic than Au ions that showed cytotoxicity at the concentrations of 25 mM.[229] This phenomenon is based on the reduced chemical activity at the surface of nanoparticles, which additionally explains why smaller nanoparticles often display elevated cytotoxicity. However, degradation of nanoparticles and release of constituent ions can lead to subacute and long-term toxicity, such as genotoxicity or carcinogenesis. Given that the application of nanoparticles relies on the increased blood circulation, specific organ accumulation, and eventual elimination, this prolonged interplay can be expected to produce undesired effects after months or even years. Unfortunately, despite the wealth of *in vitro* and *in vivo* experimental data on the acute toxicity of nanoparticles, most long-term evaluations are limited to 13−14 weeks.[230]

Exploiting the advantages of nanosystems in the design of theranostics, the immense variety of these materials as well as administration routes, frequency, and dose should be taken into account when it comes to toxicity evaluations.[231,232] While the physicochemical characteristics are the first parameters determining the developments in the initial phase, a deep understanding of the toxicity mechanisms that are intrinsically different for nanoparticles compared to small molecular drugs/contrast agents may lead to fair predictions for the *in vivo* behavior of final formulations. This approach requires specialized toxicity assays for each phase of the development process, which will facilitate the acceptance of the designed theranostics in clinics. Finally, the growing variety of smart *in vitro*, *in silico*, and *in vivo* models closer to human pathologies will provide valuable information about the long-term effects of the new theranostic probes and facilitate their translation to the clinic.

5. CONCLUSIONS AND FUTURE PERSPECTIVES

In summary, polysaccharide-based multimodal theranostic systems exhibit significant benefits compared to the system designed for either therapeutics delivery or imaging. Here, the use of polysaccharides in combination with contrast agents provides the opportunity for loading different therapeutics (such as drug and gene) inside the natural polymer matrix to achieve imaging-guided therapy. In recent years, with the significant advancements in imaging instrumentation and development of new contrast agents, the area of theranostics has seen significant progress. However, there are still some limitations which need to be addressed at the laboratory level to achieve the successful use of developed theranostics at the clinical level.

Biocompatibility of theranostic systems is a prime requirement to ensure its widespread use. In cases where synthetic polymers are used to design theranostics, their degradation rate and the toxicity caused by the degraded products are major concerns which should be investigated along with finding an alternative solution. In this regard, polysaccharides present themselves as potential candidates owing to their inherent biocompatibility. The post-modification of polysaccharides in a controlled manner to achieve different chemical functionalities and their combination with natural materials from the human body itself could pave new pathways in the area of theranostics.

Another point of prime importance while designing a theranostic system is the target specificity. Research performed at the laboratory scale to fabricate a new theranostic system or to modify an existing theranostic system requires focusing the attention on developing strategies to make them target site-specific. In this regard, *in vivo* distribution of theranostic system should be investigated in detail. In this way, both contrast agent and drug could be delivered precisely to the diseased cells without harming the healthy cells.

Addressing the long- and short-term toxicity issues of contrast agents is also a vital area which needs attention. Working at the minimal required dose of contrast agent could be one such strategy that can offer a solution to the toxicity issue. With advancement in the field of microfluidics, real-time information on the cellular response along with investigation on the contrast property of the imaging media could be recorded. As the data obtained by microfluidic chips imitates the 3D microenvironment of targeted tissues, this will give a dedicated assessment of the minimal amount to be used. Another strategy that could be used to minimize the toxicity of

https://doi.org/10.1021/acsbiomaterials.1c01631
ACS Biomater. Sci. Eng. 2022, 8, 2281−2306

contrast media is the use of biomolecules and green chemistry-based synthesis. This will reduce the use of harmful chemicals for fabricating contrast agents and will aid in reducing the toxic effects of contrast media.

Further, thorough research investigation is required in terms of doses of theranostics having contrast agents and drugs along with the gap between the doses. This will be ultimately influenced by the amount of contrast agent and drug that are loaded in the developed theranostic system. This area requires significant research with immediate attention as optimization of the contrast agent and drug amount in theranostics is very crucial for accomplishing simultaneous and efficient individual actions. For example, the use of iodinated contrast agents requires larger amounts to compensate for their faster excretion time. This higher amount may help in achieving images with better contrast, but it becomes problematic in terms of potential toxicity when CT scans at regular intervals are required for a patient to monitor the treatment progress. To address this, research has been performed where iodinated molecules have been attached to polymers or NPs.[136] However, these systems require significant efforts to improve their efficiency by maximizing their performance and minimizing their toxicity.

In short, development of theranostic systems is an interdisciplinary area requiring expertise from chemistry, material science and engineering, nanotechnology, and medicine. Hence, several experts from different fields are now joining together to develop novel theranostic systems, with maximum clinical efficiency and minimum side effects, which will help in further improving human health in the near future.

AUTHOR INFORMATION

Corresponding Author

Garima Agrawal − *School of Basic Sciences, Indian Institute of Technology, Mandi, Himachal Pradesh 175075, India;* orcid.org/0000-0002-3391-2378; Email: garima@iitmandi.ac.in

Authors

Aastha Gupta − *School of Basic Sciences, Indian Institute of Technology, Mandi, Himachal Pradesh 175075, India*

Ankur Sood − *School of Basic Sciences, Indian Institute of Technology, Mandi, Himachal Pradesh 175075, India*

Erwin Fuhrer − *School of Computing and Electrical Engineering, Indian Institute of Technology, Mandi, Himachal Pradesh 175075, India*

Kristina Djanashvili − *Department of Biotechnology, Delft University of Technology, 2629 HZ Delft, The Netherlands;* orcid.org/0000-0003-1511-015X

Complete contact information is available at: https://pubs.acs.org/10.1021/acsbiomaterials.1c01631

Author Contributions

[⊥]A.G. and A.S. are co-first authors. E.F. and K.D. contributed equally.

Notes

The authors declare no competing financial interest.

ACKNOWLEDGMENTS

Support from Department of Science & Technology, GOI (DST/INSPIRE/04/2015/003220) and IIT Mandi (Seed grant: IITM/SG/GA/72) is highly acknowledged.

REFERENCES

(1) Sauraj; Kumar, V.; Kumar, B.; Priyadarshi, R.; Deeba, F.; Kulshreshtha, A.; Kumar, A.; Agrawal, G.; Gopinath, P.; Negi, Y. S. Redox Responsive Xylan-SS-Curcumin Prodrug Nanoparticles for Dual Drug Delivery in Cancer Therapy. *Mater. Sci. Eng., C* **2020**, *107*, 110356.

(2) Agrawal, G.; Agrawal, R. Functional Microgels: Recent Advances in Their Biomedical Applications. *Small* **2018**, *14* (39), 1801724.

(3) Agrawal, G.; Agrawal, R. Janus Nanoparticles: Recent Advances in Their Interfacial and Biomedical Applications. *ACS Appl. Nano Mater.* **2019**, *2* (4), 1738−1757.

(4) Levine, R.; Krenning, E. P. Clinical History of the Theranostic Radionuclide Approach to Neuroendocrine Tumors and Other Types of Cancer: Historical Review Based on an Interview of Eric P. Krenning by Rachel Levine. *J. Nucl. Med.* **2017**, *58*, 3S−9S.

(5) Kelkar, S. S.; Reineke, T. M. Theranostics: Combining Imaging and Therapy. *Bioconjugate Chem.* **2011**, *22* (10), 1879−1903.

(6) Agrawal, G.; Agrawal, R.; Pich, A. Dual Responsive Poly(N-vinylcaprolactam) Based Degradable Microgels for Drug Delivery. *Part. Part. Syst. Charact.* **2017**, *34* (11), 1700132.

(7) Grossen, P.; Witzigmann, D.; Sieber, S.; Huwyler, J. PEG-PCL-Based Nanomedicines: A Biodegradable Drug Delivery System and Its Application. *J. Controlled Release* **2017**, *260*, 46−60.

(8) Perinelli, D. R.; Cespi, M.; Bonacucina, G.; Palmieri, G. F. PEGylated Polylactide (PLA) and Poly (lactic-co-glycolic acid) (PLGA) Copolymers for the Design of Drug Delivery Systems. *J. Pharm. Investig.* **2019**, *49* (4), 443−458.

(9) Xu, C.; Yan, Y.; Tan, J.; Yang, D.; Jia, X.; Wang, L.; Xu, Y.; Cao, S.; Sun, S. Biodegradable Nanoparticles of Polyacrylic Acid−Stabilized Amorphous $CaCO_3$ for Tunable pH-Responsive Drug Delivery and Enhanced Tumor Inhibition. *Adv. Funct. Mater.* **2019**, *29* (24), 1808146.

(10) Agrawal, G.; Wang, J.; Brüster, B.; Zhu, X.; Möller, M.; Pich, A. Degradable Microgels Synthesized Using Reactive Polyvinylalkoxysiloxanes as Crosslinkers. *Soft Matter* **2013**, *9* (22), 5380−5390.

(11) Deb, A.; R, V. Natural and Synthetic Polymer for Graphene Oxide Mediated Anticancer Drug Delivery-A Comparative Study. *Int. J. Biol. Macromol.* **2018**, *107*, 2320−2333.

(12) Agrawal, G.; Samal, S. K.; Sethi, S. K.; Manik, G.; Agrawal, R. Microgel/Silica Hybrid Colloids: Bioinspired Synthesis and Controlled Release Application. *Polymer* **2019**, *178*, 121599.

(13) Sood, A.; Gupta, A.; Agrawal, G. Recent Advances in Polysaccharides Based Biomaterials for Drug Delivery and Tissue Engineering Applications. *Carbohydr. Polym. Technol. Appl.* **2021**, *2*, 100067.

(14) Khan, T.; Date, A.; Chawda, H.; Patel, K. Polysaccharides as Potential Anticancer Agents—A Review of Their Progress. *Carbohydr. Polym.* **2019**, *210*, 412−428.

(15) Zhang, N.; Chen, H.; Ma, L.; Zhang, Y. Physical Modifications of Polysaccharide from *Inonotus obliquus* and the Antioxidant Properties. *Int. J. Biol. Macromol.* **2013**, *54*, 209−215.

(16) Liu, Q.; Duan, B.; Xu, X.; Zhang, L. Progress in Rigid Polysaccharide-Based Nanocomposites with Therapeutic Functions. *J. Mater. Chem., B* **2017**, *5* (29), 5690−5713.

(17) Yang, X.; Shi, X.; D'arcy, R.; Tirelli, N.; Zhai, G. Amphiphilic Polysaccharides as Building Blocks for Self-Assembled Nanosystems: Molecular Design and Application in Cancer and Inflammatory Diseases. *J. Controlled Release* **2018**, *272*, 114−144.

(18) Rogina, A. Electrospinning Process: Versatile Preparation Method for Biodegradable and Natural Polymers and Biocomposite Systems Applied in Tissue Engineering and Drug Delivery. *Appl. Surf. Sci.* **2014**, *296*, 221−230.

(19) Arya, G.; Das, M.; Sahoo, S. K. Evaluation of Curcumin Loaded Chitosan/PEG Blended PLGA Nanoparticles for Effective Treatment of Pancreatic Cancer. *Biomed. Pharmacother.* **2018**, *102*, 555−566.
(20) Badran, M. M.; Mady, M. M.; Ghannam, M. M.; Shakeel, F. Preparation and Characterization of Polymeric Nanoparticles Surface Modified with Chitosan for Target Treatment of Colorectal Cancer. *Int. J. Biol. Macromol.* **2017**, *95*, 643−649.
(21) Luk, B. T.; Zhang, L. Current Advances in Polymer-Based Nanotheranostics for Cancer Treatment and Diagnosis. *ACS Appl. Mater. Interfaces* **2014**, *6* (24), 21859−21873.
(22) Pearce, A. K.; Simpson, J. D.; Fletcher, N. L.; Houston, Z. H.; Fuchs, A. V.; Russell, P. J.; Whittaker, A. K.; Thurecht, K. J. Localised Delivery of Doxorubicin to Prostate Cancer Cells Through a PSMA-Targeted Hyperbranched Polymer Theranostic. *Biomaterials* **2017**, *141*, 330−339.
(23) Yang, Y.; Fan, X.; Li, L.; Yang, Y.; Nuernisha, A.; Xue, D.; He, C.; Qian, J.; Hu, Q.; Chen, H. Semiconducting Polymer Nanoparticles as Theranostic System for Near-Infrared-II Fluorescence Imaging and Photothermal Therapy under Safe Laser Fluence. *ACS Nano* **2020**, *14* (2), 2509−2521.
(24) Jaymand, M. Chemically Modified Natural Polymer-Based Theranostic Nanomedicines: Are They the Golden Gate Toward a *de Novo* Clinical Approach Against Cancer? *ACS Biomater. Sci. Eng.* **2020**, *6* (1), 134−166.
(25) Swierczewska, M.; Han, H. S.; Kim, K.; Park, J. H.; Lee, S. Polysaccharide-Based Nanoparticles for Theranostic Nanomedicine. *Adv. Drug Delivery Rev.* **2016**, *99*, 70−84.
(26) Sträter, A.; Huber, A.; Rudolph, J.; Berndt, M.; Rasper, M.; Rummeny, E. J.; Nadjiri, J. 4D-Flow MRI: Technique and Applications. *RoFo: Fortschritte auf dem Gebiete der Rontgenstrahlen und der Nuklearmedizin* **2018**, *190* (11), 1025−1035.
(27) Salama, G. R.; Heier, L. A.; Patel, P.; Ramakrishna, R.; Magge, R.; Tsiouris, A. J. Diffusion Weighted/Tensor Imaging, Functional MRI and Perfusion Weighted Imaging in Glioblastoma-Foundations and Future. *Front. Neurol.* **2018**, *8*, 660.
(28) Winter, L.; Oberacker, E.; Paul, K.; Ji, Y.; Oezerdem, C.; Ghadjar, P.; Thieme, A.; Budach, V.; Wust, P.; Niendorf, T. Magnetic Resonance Thermometry: Methodology, Pitfalls and Practical Solutions. *Int. J. Hyperthermia* **2016**, *32* (1), 63−75.
(29) Loued-Khenissi, L.; Döll, O.; Preuschoff, K. An Overview of Functional Magnetic Resonance Imaging Techniques for Organizational Research. *Organ. Res. Methods* **2019**, *22* (1), 17−45.
(30) Shokrollahi, H. Contrast Agents for MRI. *Mater. Sci. Eng., C* **2013**, *33* (8), 4485−4497.
(31) Wahsner, J.; Gale, E. M.; Rodríguez-Rodríguez, A.; Caravan, P. Chemistry of MRI Contrast Agents: Current Challenges and New Frontiers. *Chem. Rev.* **2019**, *119* (2), 957−1057.
(32) Xiao, Y.-D.; Paudel, R.; Liu, J.; Ma, C.; Zhang, Z.-S.; Zhou, S.-K. MRI Contrast Agents: Classification and Application. *Int. J. Mol. Med.* **2016**, *38* (5), 1319−1326.
(33) Zhou, Z.; Qutaish, M.; Han, Z.; Schur, R. M.; Liu, Y.; Wilson, D. L.; Lu, Z.-R. MRI Detection of Breast Cancer Micrometastases with a Fibronectin-Targeting Contrast Agent. *Nat. Commun.* **2015**, *6* (1), 1−11.
(34) Peng, X.-H.; Qian, X.; Mao, H.; Wang, A. Y.; Chen, Z. G.; Nie, S.; Shin, D. M. Targeted Magnetic Iron Oxide Nanoparticles for Tumor Imaging and Therapy. *Int. J. Nanomed.* **2008**, *3* (3), 311.
(35) Nan, X.; Lai, W.; Li, D.; Tian, J.; Hu, Z.; Fang, Q. Biocompatibility of Bacterial Magnetosomes as MRI Contrast Agent: A Long-Term *In Vivo* Follow-Up Study. *Nanomaterials (Basel)* **2021**, *11* (5), 1235.
(36) Oros, A.-M.; Shah, N. J. Hyperpolarized Xenon in NMR and MRI. *Phys. Med. Biol.* **2004**, *49* (20), R105.
(37) Roos, J. E.; McAdams, H. P.; Kaushik, S. S.; Driehuys, B. Hyperpolarized Gas MR Imaging: Technique and Applications. *Magn. Reson. Imaging Clin.* **2015**, *23* (2), 217−229.
(38) Hiriyannaiah, H. P. X-ray Computed Tomography for Medical Imaging. *IEEE signal Process.Mag.* **1997**, *14* (2), 42−59.
(39) Kalender, W. A. X-ray Computed Tomography. *Phys. Med. Biol.* **2006**, *51* (13), R29.
(40) Anuar, M. K.; Harun, A.; Razak, K. A.; Rahman, W. CT Contrast Agent of Platinum Nanodendrites: Preliminary Study. *J. Phys. Conf. Ser.* **2019**, *1248*, No. 012010.
(41) Lusic, H.; Grinstaff, M. W. X-ray-Computed Tomography Contrast Agents. *Chem. Rev.* **2013**, *113* (3), 1641−1666.
(42) Michael, G. X-ray Computed Tomography. *Phys. Educ.* **2001**, *36* (6), 442.
(43) Annexes A−D. *Ann. ICRP* **2009**, *39* (2), 47−70.
(44) Jackson, P. A.; Rahman, W. N. W. A.; Wong, C. J.; Ackerly, T.; Geso, M. Potential Dependent Superiority of Gold Nanoparticles in Comparison to Iodinated Contrast Agents. *Eur. J. Radiol.* **2010**, *75* (1), 104−109.
(45) Gerber, A.; Bundschuh, M.; Klingelhofer, D.; Groneberg, D. A. Gold Nanoparticles: Recent Aspects for Human Toxicology. *J. Occup. Med. Toxicol.* **2013**, *8* (1), 32.
(46) Senut, M. C.; Zhang, Y.; Liu, F.; Sen, A.; Ruden, D. M.; Mao, G. Size-Dependent Toxicity of Gold Nanoparticles on Human Embryonic Stem Cells and Their Neural Derivatives. *Small* **2016**, *12* (5), 631−646.
(47) Kong, X.; Sheng, H. X.; Lu, G. M.; Meinel, F. G.; Dyer, K. T.; Schoepf, U. J.; Zhang, L. J. Xenon-Enhanced Dual-Energy CT Lung Ventilation Imaging: Techniques and Clinical Applications. *Am. J. Roentgenol.* **2014**, *202* (2), 309−317.
(48) Molecular Imaging in Cardiology. In *Molecular Imaging: Radiopharmaceuticals for PET and SPECT*; Springer: Berlin Heidelberg, 2009; 299−323.
(49) Bateman, T. M. Advantages and Disadvantages of PET and SPECT in a Busy Clinical Practice. *J. Nucl. Cardiol.* **2012**, *19* (1), 3−11.
(50) Pimlott, S. L.; Sutherland, A. Molecular Tracers for the PET and SPECT Imaging of Disease. *Chem. Soc. Rev.* **2011**, *40* (1), 149−162.
(51) Contreras Ortiz, S. H.; Chiu, T.; Fox, M. D. Ultrasound Image Enhancement: A Review. *Biomed. Signal Process. Control* **2012**, *7* (5), 419−428.
(52) Paefgen, V.; Doleschel, D.; Kiessling, F. Evolution of Contrast Agents for Ultrasound Imaging and Ultrasound-Mediated Drug Delivery. *Front. Pharmacol.* **2015**, *6*, 197.
(53) Frinking, P.; Segers, T.; Luan, Y.; Tranquart, F. Three Decades of Ultrasound Contrast Agents: A Review of the Past, Present and Future Improvements. *Ultrasound Med. Biol.* **2020**, *46* (4), 892−908.
(54) Faez, T.; Emmer, M.; Kooiman, K.; Versluis, M.; van der Steen, A. F.; de Jong, N. 20 Years of Ultrasound Contrast Agent Modeling. *IEEE Trans. Ultrason. Ferroelectr. Freq. Control* **2013**, *60* (1), 7−20.
(55) Raman, R.; Sasisekharan, V.; Sasisekharan, R. Structural Insights into Biological Roles of Protein-Glycosaminoglycan Interactions. *Chem. Biol.* **2005**, *12* (3), 267−277.
(56) Swierczewska, M.; Han, H. S.; Kim, K.; Park, J. H.; Lee, S. Polysaccharide-Based Nanoparticles for Theranostic Nanomedicine. *Adv. Drug Delivery Rev.* **2016**, *99*, 70−84.
(57) Miao, T.; Wang, J.; Zeng, Y.; Liu, G.; Chen, X. Polysaccharide-Based Controlled Release Systems for Therapeutics Delivery and Tissue Engineering: From Bench to Bedside. *Adv. Sci.* **2018**, *5* (4), 1700513.
(58) Wang, J.; Li, Y.; Nie, G. Multifunctional Biomolecule Nanostructures for Cancer Therapy. *Nat. Rev. Mater.* **2021**, *6*, 766−783.
(59) Guo, J.; Rahme, K.; He, Y.; Li, L.-L.; Holmes, J. D.; O'Driscoll, C. M. Gold Nanoparticles Enlighten the Future of Cancer Theranostics. *Int. J. Nanomed.* **2017**, *12*, 6131.
(60) Wang, H.; Li, X.; Tse, B. W.-C.; Yang, H.; Thorling, C. A.; Liu, Y.; Touraud, M.; Chouane, J. B.; Liu, X.; Roberts, M. S.; Liang, X. Indocyanine Green-Incorporating Nanoparticles for Cancer Theranostics. *Theranostics* **2018**, *8* (5), 1227−1242.
(61) Zheng, X.-C.; Ren, W.; Zhang, S.; Zhong, T.; Duan, X.-C.; Yin, Y.-F.; Xu, M.-Q.; Hao, Y.-L.; Li, Z.-T.; Li, H.; Liu, M.; Li, Z.-Y.; Zhang, X. The Theranostic Efficiency of Tumor-Specific, pH-

https://doi.org/10.1021/acsbiomaterials.1c01631
ACS Biomater. Sci. Eng. 2022, 8, 2281−2306

Responsive, Peptide-Modified, Liposome-Containing Paclitaxel and Superparamagnetic Iron Oxide Nanoparticles. *Int. J. Nanomed.* **2018**, *13*, 1495−1504.
(62) Yang, Y.; Jing, L.; Li, X.; Lin, L.; Yue, X.; Dai, Z. Hyaluronic Acid Conjugated Magnetic Prussian Blue@Quantum Dot Nanoparticles for Cancer Theranostics. *Theranostics* **2017**, *7* (2), 466−481.
(63) Patel, K. D.; Singh, R. K.; Kim, H.-W. Carbon-Based Nanomaterials as an Emerging Platform for Theranostics. *Mater. Horiz.* **2019**, *6* (3), 434−469.
(64) Zeng, Y.; Xiang, Y.; Sheng, R.; Tomás, H.; Rodrigues, J.; Gu, Z.; Zhang, H.; Gong, Q.; Luo, K. Polysaccharide-Based Nanomedicines for Cancer Immunotherapy: A Review. *Bioact. Mater.* **2021**, *6* (10), 3358−3382.
(65) Fathi, M.; Majidi, S.; Zangabad, P. S.; Barar, J.; Erfan-Niya, H.; Omidi, Y. Chitosan-Based Multifunctional Nanomedicines and Theranostics for Targeted Therapy of Cancer. *Med. Res. Rev.* **2018**, *38* (6), 2110−2136.
(66) Peng, N.; Ding, X.; Wang, Z.; Cheng, Y.; Gong, Z.; Xu, X.; Gao, X.; Cai, Q.; Huang, S.; Liu, Y. Novel Dual Responsive Alginate-Based Magnetic Nanogels for Onco-Theranostics. *Carbohydr. Polym.* **2019**, *204*, 32−41.
(67) Sun, W.; Zhang, J.; Zhang, C.; Wang, P.; Peng, C.; Shen, M.; Shi, X. Construction of Hybrid Alginate Nanogels Loaded with Manganese Oxide Nanoparticles for Enhanced Tumor Magnetic Resonance Imaging. *ACS Macro Lett.* **2018**, *7* (2), 137−142.
(68) Alkahtane, A. A.; Alghamdi, H. A.; Aljasham, A. T.; Alkahtani, S. A Possible Theranostic Approach of Chitosan-Coated Iron Oxide Nanoparticles Against Human Colorectal Carcinoma (HCT-116) Cell Line. *Saudi J. Biol. Sci.* **2022**, *29* (1), 154−160.
(69) Sood, A.; Arora, V.; Kumari, S.; Sarkar, A.; Kumaran, S. S.; Chaturvedi, S.; Jain, T. K.; Agrawal, G. Imaging Application and Radiosensitivity Enhancement of Pectin Decorated Multifunctional Magnetic Nanoparticles in Cancer Therapy. *Int. J. Biol. Macromol.* **2021**, *189*, 443−454.
(70) Sood, A.; Arora, V.; Shah, J.; Kotnala, R. K.; Jain, T. K. Multifunctional Gold Coated Iron Oxide Core-Shell Nanoparticles Stabilized Using Thiolated Sodium Alginate for Biomedical Applications. *Mater. Sci. Eng. C* **2017**, *80*, 274−281.
(71) Das, M.; Oyarzabal, E. A.; Chen, L.; Lee, S.-H.; Shah, N.; Gerlach, G.; Zhang, W.; Chao, T.-H. H.; Berge, N.V. D.; Liu, C.; Donley, C.; Montgomery, S. A.; Shih, Y.-Y. I. One-Pot Synthesis of Carboxymethyl-Dextran Coated Iron Oxide Nanoparticles (CION) for Preclinical fMRI and MRA Applications. *NeuroImage* **2021**, *238*, 118213.
(72) Unterweger, H.; Dézsi, L.; Matuszak, J.; Janko, C.; Poettler, M.; Jordan, J.; Bäuerle, T.; Szebeni, J.; Fey, T.; Boccaccini, A. R. Dextran-Coated Superparamagnetic Iron Oxide Nanoparticles for Magnetic Resonance Imaging: Evaluation of Size-Dependent Imaging Properties, Storage, Stability and Safety. *Int. J. Nanomed.* **2018**, *13*, 1899−1915.
(73) Lu, R.; Zhang, Y.; Tao, H.; Zhou, L.; Li, H.; Chen, T.; Zhang, P.; Lu, Y.; Chen, S. Gadolinium-Hyaluronic Acid Nanoparticles as an Efficient and Safe Magnetic Resonance Imaging Contrast Agent for Articular Cartilage Injury Detection. *Bioact. Mater.* **2020**, *5* (4), 758−767.
(74) Guo, C.; Sun, L.; Cai, H.; Duan, Z.; Zhang, S.; Gong, Q.; Luo, K.; Gu, Z. Gadolinium-Labeled Biodegradable Dendron−Hyaluronic Acid Hybrid and Its Subsequent Application as a Safe and Efficient Magnetic Resonance Imaging Contrast Agent. *ACS Appl. Mater. Interfaces* **2017**, *9* (28), 23508−23519.
(75) Thomas, R. G.; Muthiah, M.; Moon, M.; Park, I.-K.; Jeong, Y. Y. SPION loaded Poly(L-lysine)/Hyaluronic Acid Micelles as MR Contrast Agent and Gene Delivery Vehicle for Cancer Theranostics. *Macromol. Res.* **2017**, *25*, 446−451.
(76) Shin, T.-H.; Kim, P. K.; Kang, S.; Cheong, J.; Kim, S.; Lim, Y.; Shin, W.; Jung, J.-Y.; Lah, J. D.; Choi, B. W.; Cheon, J. High-Resolution T_1 MRI *via* Renally Clearable Dextran Nanoparticles With an Iron Oxide Shell. *Nat. Biomed. Eng.* **2021**, *5*, 252−263.
(77) Abbasi Pour, S.; Shaterian, H. R.; Afradi, M.; Yazdani-Elah-Abadi, A. Carboxymethyl Cellulose (CMC)-Loaded Co-Cu Doped Manganese Ferrite Nanorods as a New Dual-Modal Simultaneous Contrast Agent for Magnetic Resonance Imaging and Nanocarrier for Drug Delivery System. *J. Magn. Magn. Mater.* **2017**, *438*, 85−94.
(78) Klemm, P. J.; Floyd, W. C., 3rd; Smiles, D. E.; Fréchet, J. M. J.; Raymond, K. N. Improving T_1 and T_2 Magnetic Resonance Imaging Contrast Agents Through the Conjugation of an Esteramide Dendrimer to High-Water-Coordination Gd(III) Hydroxypyridinone Complexes. *Contrast Media Mol. Imaging* **2012**, *7* (1), 95−99.
(79) Sun, W.; Thies, S.; Zhang, J.; Peng, C.; Tang, G.; Shen, M.; Pich, A.; Shi, X. Gadolinium-Loaded Poly (N-vinylcaprolactam) Nanogels: Synthesis, Characterization, and Application for Enhanced Tumor MR Imaging. *ACS Appl. Mater. Interfaces* **2017**, *9* (4), 3411−3418.
(80) Fuchs, A. V.; Bapat, A. P.; Cowin, G. J.; Thurecht, K. J. Switchable ^{19}F MRI Polymer Theranostics: Towards *In Situ* Quantifiable Drug Release. *Polym. Chem.* **2017**, *8* (34), 5157−5166.
(81) Hrkach, J.; Von Hoff, D.; Ali, M. M.; Andrianova, E.; Auer, J.; Campbell, T.; De Witt, D.; Figa, M.; Figueiredo, M.; Horhota, A. Preclinical Development and Clinical Translation of a PSMA-Targeted Docetaxel Nanoparticle with a Differentiated Pharmacological Profile. *Sci. Transl. Med.* **2012**, *4* (128), 128ra139−128ra139.
(82) Kumari, A.; Yadav, S. K.; Yadav, S. C. Biodegradable Polymeric Nanoparticles Based Drug Delivery Systems. *Colloids Surf. B: Biointerfaces* **2010**, *75* (1), 1−18.
(83) Liu, J.; Zheng, J.; Nie, H.; Zhang, D.; Cao, D.; Xing, Z.; Li, B.; Jia, L. Molybdenum Disulfide-Based Hyaluronic Acid-Guided Multifunctional Theranostic Nanoplatform for Magnetic Resonance Imaging and Synergetic Chemo-Photothermal Therapy. *J. Colloid Interface Sci.* **2019**, *548*, 131−144.
(84) Cavalli, R.; Argenziano, M.; Vigna, E.; Giustetto, P.; Torres, E.; Aime, S.; Terreno, E. Preparation and *In Vitro* Characterization of Chitosan Nanobubbles as Theranostic Agents. *Colloids Surf. B: Biointerfaces* **2015**, *129*, 39−46.
(85) Podgórna, K.; Szczepanowicz, K.; Piotrowski, M.; Gajdošová, M.; Štěpánek, F.; Warszyński, P. Gadolinium Alginate Nanogels for Theranostic Applications. *Colloids Surf. B: Biointerfaces* **2017**, *153*, 183−189.
(86) Wang, C.; Ravi, S.; Garapati, U. S.; Das, M.; Howell, M.; Mallela, J.; Alwarappan, S.; Mohapatra, S. S.; Mohapatra, S. Multifunctional Chitosan Magnetic-Graphene (CMG) Nanoparticles: A Theranostic Platform for Tumor-Targeted co-Delivery of Drugs, Genes and MRI Contrast Agents. *J. Mater. Chem., B* **2013**, *1* (35), 4396−4405.
(87) Baktash, M. S.; Zarrabi, A.; Avazverdi, E.; Reis, N. M. Development and Optimization of a New Hybrid Chitosan-Grafted Graphene Oxide/Magnetic Nanoparticle System for Theranostic Applications. *J. Mol. Liq.* **2021**, *322*, 114515.
(88) Gholami, L.; Tafaghodi, M.; Abbasi, B.; Daroudi, M.; Kazemi Oskuee, R. Preparation of Superparamagnetic Iron Oxide/Doxorubicin Loaded Chitosan Nanoparticles as a Promising Glioblastoma Theranostic Tool. *J. Cell. Physiol.* **2019**, *234* (2), 1547−1559.
(89) Arora, V.; Sood, A.; Kumari, S.; Kumaran, S. S.; Jain, T. K. Hydrophobically Modified Sodium Alginate Conjugated Plasmonic Magnetic Nanocomposites for Drug Delivery & Magnetic Resonance Imaging. *Mater. Today Commun.* **2020**, *25*, 101470.
(90) van Elk, M.; Lorenzato, C.; Ozbakir, B.; Oerlemans, C.; Storm, G.; Nijsen, F.; Deckers, R.; Vermonden, T.; Hennink, W. E. Alginate Microgels Loaded with Temperature Sensitive Liposomes for Magnetic Resonance Imageable Drug Release and Microgel Visualization. *Eur. Polym. J.* **2015**, *72*, 620−631.
(91) Nejadshafiee, V.; Naeimi, H.; Goliaei, B.; Bigdeli, B.; Sadighi, A.; Dehghani, S.; Lotfabadi, A.; Hosseini, M.; Nezamtaheri, M. S.; Amanlou, M.; Sharifzadeh, M.; Khoobi, M. Magnetic Bio-Metal−Organic Framework Nanocomposites Decorated with Folic Acid Conjugated Chitosan as a Promising Biocompatible Targeted Theranostic System for Cancer Treatment. *Mater. Sci. Eng., C* **2019**, *99*, 805−815.

https://doi.org/10.1021/acsbiomaterials.1c01631
ACS Biomater. Sci. Eng. 2022, 8, 2281−2306

(92) Li, S.-Y.; Zhao, L.-P.; Zheng, R.-R.; Fan, G.-L.; Liu, L.-S.; Zhou, X.; Chen, X.-T.; Qiu, X.-Z.; Yu, X.-Y.; Cheng, H. Tumor Microenvironment Adaptable Nanoplatform for O_2 Self-Sufficient Chemo/Photodynamic Combination Therapy. *Part. Part. Syst. Charact.* **2020**, *37* (3), 1900496.
(93) Zhao, L.; Qiu, G.; Wang, K.; Chen, H.; Ruan, F.; Liu, N.; Deng, Z.; Yao, Y.; Guo, D.; Wang, D.; Sha, L.; Kong, X.; Liu, W.; Zhang, Y. A Nano-Integrated Diagnostic and Therapeutic Platform with Oxidation−Reduction Reactions in Tumor Microenvironments. *Nanoscale Adv.* **2020**, *2* (5), 2192−2202.
(94) Wu, Y.; Zhang, R.; Tran, H. D. N.; Kurniawan, N. D.; Moonshi, S. S.; Whittaker, A. K.; Ta, H. T. Chitosan Nanococktails Containing Both Ceria and Superparamagnetic Iron Oxide Nanoparticles for Reactive Oxygen Species-Related Theranostics. *ACS Appl. Nano Mater.* **2021**, *4* (4), 3604−3618.
(95) Zhao, X.; Shen, R.; Bao, L.; Wang, C.; Yuan, H. Chitosan Derived Glycolipid Nanoparticles for Magnetic Resonance Imaging Guided Photodynamic Therapy of Cancer. *Carbohydr. Polym.* **2020**, *245*, 116509.
(96) Hemalatha, T.; Prabu, P.; Gunadharini, D. N.; Gowthaman, M. K. Fabrication and Characterization of Dual Acting Oleyl Chitosan Functionalised Iron Oxide/Gold Hybrid Nanoparticles for MRI and CT Imaging. *Int. J. Biol. Macromol.* **2018**, *112*, 250−257.
(97) Tran, T. T.-D.; Tran, P. H.-L.; Amin, H. H.; Lee, B.-J. Biodistribution and *In Vivo* Performance of Fattigation-Platform Theranostic Nanoparticles. *Mater. Sci. Eng., C* **2017**, *79*, 671−678.
(98) Wang, G.; Gao, S.; Tian, R.; Miller-Kleinhenz, J.; Qin, Z.; Liu, T.; Li, L.; Zhang, F.; Ma, Q.; Zhu, L. Theranostic Hyaluronic Acid−Iron Micellar Nanoparticles for Magnetic-Field-Enhanced *In Vivo* Cancer Chemotherapy. *ChemMedChem.* **2018**, *13* (1), 78−86.
(99) Yang, H.; Chen, Y.; Chen, Z.; Geng, Y.; Xie, X.; Shen, X.; Li, T.; Li, S.; Wu, C.; Liu, Y. Chemo-Photodynamic Combined Gene Therapy and Dual-Modal Cancer Imaging Achieved by pH-Responsive Alginate/Chitosan Multilayer-Modified Magnetic Mesoporous Silica Nanocomposites. *Biomater. Sci.* **2017**, *5* (5), 1001−1013.
(100) Du, F.; Wu, Y.; Du, F.; Zhang, L.; Feng, W.; Zhao, L.; Cai, R.; Xu, L.; Bian, G.; Li, J.; Zou, S.; Gong, A.; Zhang, M. Construction of Catechol-Grafted Chitosan Alginate/Barium Sulfate Microcapsules for Computed Tomography Real-Time Imaging and Gastroretentive Drug Delivery. *Int. J. Nanomed.* **2019**, *14*, 6001−6018.
(101) Choi, D.; Jeon, S.; You, D. G.; Um, W.; Kim, J.-Y.; Yoon, H. Y.; Chang, H.; Kim, D.-E.; Park, J. H.; Kim, H.; Kim, K. Iodinated Echogenic Glycol Chitosan Nanoparticles for X-ray CT/US Dual Imaging of Tumor. *Nanotheranostics* **2018**, *2* (2), 117−127.
(102) Yu, S.; Wen, R.; Wang, H.; Zha, Y.; Qiu, L.; Li, B.; Xue, W.; Ma, D. Chitosan-graft-Poly(L-lysine) Dendron-Assisted Facile Self-Assembly of Au Nanoclusters for Enhanced X-ray Computer Tomography Imaging and Precise MMP-9 Plasmid shRNA Delivery. *Chem. Mater.* **2019**, *31* (11), 3992−4007.
(103) Sarkar, A.; Roy, S.; Sanpui, P.; Jaiswal, A. Plasmonic Gold Nanorattle Impregnated Chitosan Nanocarrier for Stimulus Responsive Theranostics. *ACS Appl. Bio Mater.* **2019**, *2* (11), 4812−4825.
(104) Niu, S.; Zhang, X.; Williams, G. R.; Wu, J.; Gao, F.; Fu, Z.; Chen, X.; Lu, S.; Zhu, L.-M. Hollow Mesoporous Silica Nanoparticles Gated by Chitosan-Copper Sulfide Composites as Theranostic Agents for the Treatment of Breast Cancer. *Acta Biomater.* **2021**, *126*, 408−420.
(105) Wang, J.; Pang, X.; Tan, X.; Song, Y.; Liu, L.; You, Q.; Sun, Q.; Tan, F.; Li, N. A Triple-Synergistic Strategy for Combinational Photo/Radiotherapy and Multi-Modality Imaging Based on Hyaluronic Acid-Hybridized Polyaniline-Coated WS_2 Nanodots. *Nanoscale* **2017**, *9* (17), 5551−5564.
(106) Wang, Y.-Y.; Wang, W.-L.; Shen, X.-C.; Zhou, B.; Chen, T.; Guo, Z.-X.; Wen, C.-C.; Jiang, B.-P.; Liang, H. Combination-Responsive MoO_{3-x}-Hybridized Hyaluronic Acid Hollow Nanospheres for Cancer Phototheranostics. *ACS Appl. Mater. Interfaces* **2018**, *10*, 42088−42101.
(107) Zhu, C.; Ma, X.; Ma, D.; Zhang, T.; Gu, N. Crosslinked Dextran Gel Microspheres with Computed Tomography Angiography and Drug Release Function. *J. Nanosci. Nanotechnol.* **2018**, *18* (4), 2931−2937.
(108) Liu, Z.; Li, Y.; Li, W.; Xiao, C.; Liu, D.; Dong, C.; Zhang, M.; Mäkilä, E.; Kemell, M.; Salonen, J.; Hirvonen, J. T.; Zhang, H.; Zhou, D.; Deng, X.; Santos, H. A. Multifunctional Nanohybrid Based on Porous Silicon Nanoparticles, Gold Nanoparticles, and Acetalated Dextran for Liver Regeneration and Acute Liver Failure Theranostics. *Adv. Mater.* **2018**, *30* (24), 1703393.
(109) Yang, H.; Wang, N.; Yang, R.; Zhang, L.; Jiang, X. Folic Acid-Decorated β-Cyclodextrin-Based Poly(ε-caprolactone)-dextran Star Polymer with Disulfide Bond-Linker as Theranostic Nanoparticle for Tumor-Targeted MRI and Chemotherapy. *Pharmaceutics* **2022**, *14* (1), 52.
(110) Lin, Y.; Wang, S.; Zhang, Y.; Gao, J.; Hong, L.; Wang, X.; Wu, W.; Jiang, X. Ultra-High Relaxivity Iron Oxide Nanoparticles Confined in Polymer Nanospheres for Tumor MR Imaging. *J. Mater. Chem. B* **2015**, *3*, 5702−5710.
(111) Dai, X.; Zhao, X.; Liu, Y.; Chen, B.; Ding, X.; Zhao, N.; Xu, F.-J. Controlled Synthesis and Surface Engineering of Janus Chitosan-Gold Nanoparticles for Photoacoustic Imaging-Guided Synergistic Gene/Photothermal Therapy. *Small* **2021**, *17* (11), 2006004.
(112) Song, L.; Zhou, X.; Dai, X.; Wang, R.; Cheng, G.; Zhao, N.; Xu, F.-J. Self-Destructible Polysaccharide Nanocomposites with Unlockable Au Nanorods for High-Performance Photothermal Therapy. *NPG Asia Mater.* **2018**, *10*, 509−521.
(113) Lee, D.-E.; Koo, H.; Sun, I.-C.; Ryu, J. H.; Kim, K.; Kwon, I. C. Multifunctional Nanoparticles for Multimodal Imaging and Theragnosis. *Chem. Soc. Rev.* **2012**, *41* (7), 2656−2672.
(114) Yu, Y.; Yang, T.; Sun, T. New Insights into the Synthesis, Toxicity and Applications of Gold Nanoparticles in CT Imaging and Treatment of Cancer. *Nanomedicine* **2020**, *15* (11), 1127−1145.
(115) Letsinger, R. L.; Elghanian, R.; Viswanadham, G.; Mirkin, C. A. Use of a Steroid Cyclic Disulfide Anchor in Constructing Gold Nanoparticle−Oligonucleotide Conjugates. *Bioconjugate Chem.* **2000**, *11* (2), 289−291.
(116) Huff, T. B.; Hansen, M. N.; Zhao, Y.; Cheng, J.-X.; Wei, A. Controlling the Cellular Uptake of Gold Nanorods. *Langmuir* **2007**, *23* (4), 1596−1599.
(117) Sun, I.-C.; Eun, D.-K.; Koo, H.; Ko, C.-Y.; Kim, H.-S.; Yi, D. K.; Choi, K.; Kwon, I. C.; Kim, K.; Ahn, C.-H. Tumor-Targeting Gold Particles for Dual Computed Tomography/Optical Cancer Imaging. *Angew. Chem., Int. Ed.* **2011**, *50* (40), 9348−9351.
(118) Sun, I.-C.; Na, J. H.; Jeong, S. Y.; Kim, D.-E.; Kwon, I. C.; Choi, K.; Ahn, C.-H.; Kim, K. Biocompatible Glycol Chitosan-Coated Gold Nanoparticles for Tumor-Targeting CT Imaging. *Pharm. Res.* **2014**, *31* (6), 1418−1425.
(119) Sun, I.-C.; Eun, D.-K.; Na, J. H.; Lee, S.; Kim, I.-J.; Youn, I.-C.; Ko, C.-Y.; Kim, H.-S.; Lim, D.; Choi, K.; Messersmith, P. B.; Park, T. G.; Kim, S. Y.; Kwon, I. C.; Kim, K.; Ahn, C.-H. Heparin-Coated Gold Nanoparticles for Liver-Specific CT Imaging. *Chem.—Eur. J.* **2009**, *15* (48), 13341−13347.
(120) Keshavarz, M.; Moloudi, K.; Paydar, R.; Abed, Z.; Beik, J.; Ghaznavi, H.; Shakeri-Zadeh, A. Alginate Hydrogel co-Loaded with Cisplatin and Gold Nanoparticles for Computed Tomography Image-Guided Chemotherapy. *J. Biomater. Appl.* **2018**, *33* (2), 161−169.
(121) Li, J.; Hu, Y.; Yang, J.; Wei, P.; Sun, W.; Shen, M.; Zhang, G.; Shi, X. Hyaluronic Acid-Modified Fe_3O_4@Au Core/Shell Nanostars for Multimodal Imaging and Photothermal Therapy of Tumors. *Biomaterials* **2015**, *38*, 10−21.
(122) Huang, X.; Teng, X.; Chen, D.; Tang, F.; He, J. The Effect of the Shape of Mesoporous Silica Nanoparticles on Cellular Uptake and Cell Function. *Biomaterials* **2010**, *31* (3), 438−448.
(123) Hu, H.; Hou, X.-J.; Wang, X.-C.; Nie, J.-J.; Cai, Q.; Xu, F.-J. Gold Nanoparticle-Conjugated Heterogeneous Polymer Brush-Wrapped Cellulose Nanocrystals Prepared by Combining Different Controllable Polymerization Techniques for Theranostic Applications. *Polym. Chem.* **2016**, *7* (18), 3107−3116.

https://doi.org/10.1021/acsbiomaterials.1c01631
ACS Biomater. Sci. Eng. 2022, 8, 2281−2306

(124) Uthaman, S.; Kim, H. S.; Revuri, V.; Min, J.-J.; Lee, Y.-k.; Huh, K. M.; Park, I.-K. Green Synthesis of Bioactive Polysaccharide-Capped Gold Nanoparticles for Lymph Node CT Imaging. *Carbohydr. Polym.* **2018**, *181*, 27−33.
(125) Du, F.; Lou, J.; Jiang, R.; Fang, Z.; Zhao, X.; Niu, Y.; Zou, S.; Zhang, M.; Gong, A.; Wu, C. Hyaluronic Acid-Functionalized Bismuth Oxide Nanoparticles for Computed Tomography Imaging-Guided Radiotherapy of Tumor. *Int. J. Nanomed.* **2017**, *12*, 5973−5992.
(126) Alqathami, M.; Blencowe, A.; Yeo, U. J.; Franich, R.; Doran, S.; Qiao, G.; Geso, M. Enhancement of Radiation Effects by Bismuth Oxide Nanoparticles for Kilovoltage X-ray Beams: A Dosimetric Study Using a Novel Multi-Compartment 3D Radiochromic Dosimeter. *J. Phys.: Conf. Ser.* **2013**, *444*, No. 012025.
(127) Rabin, O.; Manuel Perez, J.; Grimm, J.; Wojtkiewicz, G.; Weissleder, R. An X-ray Computed Tomography Imaging Agent Based on Long-Circulating Bismuth Sulphide Nanoparticles. *Nat. Mater.* **2006**, *5* (2), 118−122.
(128) Li, Z.; Hu, Y.; Howard, K. A.; Jiang, T.; Fan, X.; Miao, Z.; Sun, Y.; Besenbacher, F.; Yu, M. Multifunctional Bismuth Selenide Nanocomposites for Antitumor Thermo-Chemotherapy and Imaging. *ACS Nano* **2016**, *10* (1), 984−997.
(129) Firouzi, M.; Poursalehi, R.; Delavari H, H.; Saba, F.; Oghabian, M. A. Chitosan Coated Tungsten Trioxide Nanoparticles as a Contrast Agent for X-ray Computed Tomography. *Int. J. Biol. Macromol.* **2017**, *98*, 479−485.
(130) Wu, Y.; Liang, Y.; Liu, Y.; Hao, Y.; Tao, N.; Li, J.; Sun, X.; Zhou, M.; Liu, Y.-N. A Bi_2S_3-Embedded Gellan Gum Hydrogel for Localized Tumor Photothermal/Antiangiogenic Therapy. *J. Mater. Chem. B* **2021**, *9*, 3224−3234.
(131) Song, Y.; Wang, Y.; Zhu, Y.; Cheng, Y.; Wang, Y.; Wang, S.; Tan, F.; Lian, F.; Li, N. Biomodal Tumor-Targeted and Redox-Responsive Bi_2Se_3 Hollow Nanocubes for MSOT/CT Imaging Guided Synergistic Low-Temperature Photothermal Radiotherapy. *Adv. Healthc. Mater.* **2019**, *8* (16), 1900250.
(132) Jin, Y.; Tang, C.; Tian, J.; Shao, B. Integration of TaO_x with Bi_2S_3 for Targeted Multimodality Breast Cancer Theranostics. *Bioconjugate Chem.* **2021**, *32*, 161−171.
(133) Wu, S.; Meng, X.; Jiang, X.; Wu, Y.; Zhai, S.; Wang, X.; Liu, Y.; Zhang, J.; Zhao, X.; Zhou, Y.; Bu, W.; Yao, Z. *Adv. Sci. (Weinh)* **2021**, *8*, No. e2002548.
(134) Wang, Y.; Cai, D.; Wu, H.; Fu, Y.; Cao, Y.; Zhang, Y.; Wu, D.; Tian, Q.; Yang, S. Functionalized Cu_3BiS_3 Nanoparticles for Dual-Modal Imaging and Targeted Photothermal/Photodynamic Therapy. *Nanoscale* **2018**, *10*, 4452−4462.
(135) Liu, Y.; Ai, K.; Liu, J.; Yuan, Q.; He, Y.; Lu, L. A High-Performance Ytterbium-Based Nanoparticulate Contrast Agent for *In Vivo* X-ray Computed Tomography Imaging. *Angew. Chem.* **2012**, *124* (6), 1466−1471.
(136) Zhu, Y.; Wang, X.; Chen, J.; Zhang, J.; Meng, F.; Deng, C.; Cheng, R.; Feijen, J.; Zhong, Z. Bioresponsive and Fluorescent Hyaluronic Acid-Iodixanol Nanogels for Targeted X-ray Computed Tomography Imaging and Chemotherapy of Breast Tumors. *J. Controlled Release* **2016**, *244*, 229−239.
(137) Lee, J.-Y.; Chung, S.-J.; Cho, H.-J.; Kim, D.-D. Iodinated Hyaluronic Acid Oligomer-Based Nanoassemblies for Tumor-Targeted Drug Delivery and Cancer Imaging. *Biomaterials* **2016**, *85*, 218−231.
(138) Liang, X.; Fang, L.; Li, X.; Zhang, X.; Wang, F. Activatable Near Infrared Dye Conjugated Hyaluronic Acid Based Nanoparticles as a Targeted Theranostic Agent for Enhanced Fluorescence/CT/Photoacoustic Imaging Guided Photothermal Therapy. *Biomaterials* **2017**, *132*, 72−84.
(139) Herth, M. M.; Barz, M.; Moderegger, D.; Allmeroth, M.; Jahn, M.; Thews, O.; Zentel, R.; Rösch, F. Radioactive Labeling of Defined HPMA-Based Polymeric Structures Using [^{18}F]FETos for *In Vivo* Imaging by Positron Emission Tomography. *Biomacromolecules* **2009**, *10* (7), 1697−1703.
(140) Boros, E.; Packard, A. B. Radioactive Transition Metals for Imaging and Therapy. *Chem. Rev.* **2019**, *119* (2), 870−901.
(141) Wei, W.; Rosenkrans, Z. T.; Liu, J.; Huang, G.; Luo, Q.-Y.; Cai, W. ImmunoPET: Concept, Design, and Applications. *Chem. Rev.* **2020**, *120* (8), 3787−3851.
(142) Schmitt, V.; Rodríguez-Rodríguez, C.; Hamilton, J. L.; Shenoi, R. A.; Schaffer, P.; Sossi, V.; Kizhakkedathu, J. N.; Saatchi, K.; Häfeli, U. O. Quantitative SPECT Imaging and Biodistribution Point to Molecular Weight Independent Tumor Uptake for Some Long-Circulating Polymer Nanocarriers. *RSC Adv.* **2018**, *8* (10), 5586−5595.
(143) Stockhofe, K.; Postema, J. M.; Schieferstein, H.; Ross, T. L. Radiolabeling of Nanoparticles and Polymers for PET Imaging. *Pharmaceuticals (Basel, Switzerland)* **2014**, *7* (4), 392−418.
(144) Sun, J.; Sun, L.; Li, J.; Xu, J.; Wan, Z.; Ouyang, Z.; Liang, L.; Li, S.; Zeng, D. A Multi-Functional Polymeric Carrier for Simultaneous Positron Emission Tomography Imaging and Combination Therapy. *Acta Biomater.* **2018**, *75*, 312−322.
(145) Dzhardimalieva, G. I.; Rabinskiy, L. N.; Kydralieva, K. A.; Uflyand, I. E. Recent Advances in Metallopolymer-Based Drug Delivery Systems. *RSC Adv.* **2019**, *9* (63), 37009−37051.
(146) Cho, E. J.; Sun, B.; Doh, K. O.; Wilson, E. M.; Torregrosa-Allen, S.; Elzey, B. D.; Yeo, Y. Intraperitoneal Delivery of Platinum with *In-Situ* Crosslinkable Hyaluronic Acid Gel for Local Therapy of Ovarian Cancer. *Biomaterials* **2015**, *37*, 312−319.
(147) Pawar, S. N.; Edgar, K. J. Alginate Derivatization: A Review of Chemistry, Properties and Applications. *Biomaterials* **2012**, *33* (11), 3279−3305.
(148) Liao, J.; Wang, B.; Huang, Y.; Qu, Y.; Peng, J.; Qian, Z. Injectable Alginate Hydrogel Cross-Linked by Calcium Gluconate-Loaded Porous Microspheres for Cartilage Tissue Engineering. *ACS Omega* **2017**, *2* (2), 443−454.
(149) d'Angelo, I.; Conte, C.; La Rotonda, M. I.; Miro, A.; Quaglia, F.; Ungaro, F. Improving the Efficacy of Inhaled Drugs in Cystic Fibrosis: Challenges and Emerging Drug Delivery Strategies. *Adv. Drug Delivery Rev.* **2014**, *75*, 92−111.
(150) Patrick, P. S.; Bear, J. C.; Fitzke, H. E.; Zaw-Thin, M.; Parkin, I. P.; Lythgoe, M. F.; Kalber, T. L.; Stuckey, D. J. Radio-Metal Cross-Linking of Alginate Hydrogels for Non-Invasive *In Vivo* Imaging. *Biomaterials* **2020**, *243*, 119930.
(151) Gholipour, N.; Akhlaghi, M.; Kheirabadi, A. M.; Beiki, D.; Geramifar, P.; Yousefnia, H.; Mazidi, M. Chelator-Free Radiolabeling of Dextran with ^{68}Ga for PET Studies. *J. Radioanal. Nucl. Chem.* **2017**, *311* (3), 1811−1817.
(152) Keliher, E. J.; Yoo, J.; Nahrendorf, M.; Lewis, J. S.; Marinelli, B.; Newton, A.; Pittet, M. J.; Weissleder, R. ^{89}Zr-Labeled Dextran Nanoparticles Allow *In Vivo* Macrophage Imaging. *Bioconjugate Chem.* **2011**, *22* (12), 2383−2389.
(153) Polyak, A.; Ross, T. L. Nanoparticles for SPECT and PET Imaging: Towards Personalized Medicine and Theranostics. *Curr. Med. Chem.* **2018**, *25* (34), 4328−4353.
(154) Weissleder, R.; Pittet, M. J. Imaging in the Era of Molecular Oncology. *Nature* **2008**, *452* (7187), 580−589.
(155) Duncan, R. Polymer Conjugates as Anticancer Nanomedicines. *Nat. Rev. Cancer* **2006**, *6* (9), 688−701.
(156) Imlimthan, S.; Khng, Y. C.; Keinänen, O.; Zhang, W.; Airaksinen, A. J.; Kostiainen, M. A.; Zeglis, B. M.; Santos, H. A.; Sarparanta, M. A Theranostic Cellulose Nanocrystal-Based Drug Delivery System with Enhanced Retention in Pulmonary Metastasis of Melanoma. *Small* **2021**, *17* (18), 2007705.
(157) Tekie, F. S.; Kiani, M.; Zakerian, A.; Pilevarian, F.; Assali, A.; Soleimani, M.; Dinarvand, R.; Arefian, E.; Atashi, A.; Amini, M.; Atyabi, F. Nano Polyelectrolyte Complexes of Carboxymethyl Dextran and Chitosan to Improve Chitosan-Mediated Delivery of miR-145. *Carbohydr. Polym.* **2017**, *159*, 66−75.
(158) Naskar, S.; Koutsu, K.; Sharma, S. Chitosan-Based Nanoparticles as Drug Delivery Systems: A Review on Two Decades of Research. *J. Drug Target* **2019**, *27* (4), 379−393.

https://doi.org/10.1021/acsbiomaterials.1c01631
ACS Biomater. Sci. Eng. 2022, 8, 2281−2306

(159) Hwang, H.; Kim, K. I.; Kwon, J.; Kim, B. S.; Jeong, H.-S.; Jang, S. J.; Oh, P.-S.; Park, H. S.; Lim, S. T.; Sohn, M.-H.; Jeong, H.-J. ^{131}I-Labeled Chitosan Hydrogels for Radioembolization: A Preclinical Study in Small Animals. *Nucl. Med. Biol.* **2017**, *52*, 16−23.
(160) Pang, F.; Li, Y.; Zhang, W.; Xia, C.; He, Q.; Li, Z.; Xiao, L.; Song, S.; Dong, P.; Zhou, H.; Shao, T.; Cai, H.; Li, L. Biodegradable ^{131}Iodine-Labeled Microspheres: Potential Transarterial Radioembolization Biomaterial for Primary Hepatocellular Carcinoma Treatment. *Adv. Healthc. Mater.* **2020**, *9* (13), 2000028.
(161) Lee, D. E.; Na, J. H.; Lee, S.; Kang, C. M.; Kim, H. N.; Han, S. J.; Kim, H.; Choe, Y. S.; Jung, K. H.; Lee, K. C.; Choi, K.; Kwon, I. C.; Jeong, S. Y.; Lee, K.-H.; Kim, K. Facile Method to Radiolabel Glycol Chitosan Nanoparticles with ^{64}Cu *via* Copper-Free Click Chemistry for MicroPET Imaging. *Mol. Pharmaceutics* **2013**, *10* (6), 2190−2198.
(162) Lee, S.; Kang, S.-W.; Ryu, J. H.; Na, J. H.; Lee, D.-E.; Han, S. J.; Kang, C. M.; Choe, Y. S.; Lee, K. C.; Leary, J. F.; Choi, K.; Lee, K.-H.; Kim, K. Tumor-Homing Glycol Chitosan-Based Optical/PET Dual Imaging Nanoprobe for Cancer Diagnosis. *Bioconjugate Chem.* **2014**, *25* (3), 601−610.
(163) Polyák, A.; Hajdu, I.; Bodnár, M.; Dabasi, G.; Jóba, R. P.; Borbély, J.; Balogh, L. Folate Receptor Targeted Self-Assembled Chitosan-Based Nanoparticles for SPECT/CT Imaging: Demonstrating a Preclinical Proof of Concept. *Int. J. Pharm.* **2014**, *474* (1−2), 91−94.
(164) Körhegyi, Z.; Rózsa, D.; Hajdu, I.; Bodnár, M.; Kertész, I.; Kerekes, K.; Kun, S.; Kollár, J.; Varga, J.; Garai, I.; Trencsényi, G.; Borbély, J. Synthesis of ^{68}Ga-Labeled Biopolymer-Based Nanoparticle Imaging Agents for Positron-Emission Tomography. *Anticancer Res.* **2019**, *39* (5), 2415−2427.
(165) Cai, X.; Jiang, Y.; Lin, M.; Zhang, J.; Guo, H.; Yang, F.; Leung, W.; Xu, C. Ultrasound-Responsive Materials for Drug/Gene Delivery. *Front. Pharmacol.* **2020**, *10* (1650), 1 DOI: 10.3389/fphar.2019.01650.
(166) Pitt, W. G.; Husseini, G. A.; Staples, B. J. Ultrasonic Drug Delivery-A General Review. *Expert Opin. Drug Delivery* **2004**, *1* (1), 37−56.
(167) Husseini, G. A.; Velluto, D.; Kherbeck, L.; Pitt, W. G.; Hubbell, J. A.; Christensen, D. A. Investigating the Acoustic Release of Doxorubicin from Targeted Micelles. *Colloids Surf. B: Biointerfaces* **2013**, *101*, 153−155.
(168) Shang, M.; Sun, X.; Guo, L.; Shi, D.; Liang, P.; Meng, D.; Zhou, X.; Liu, X.; Zhao, Y.; Li, J. pH- and Ultrasound-Responsive Paclitaxel-Loaded Carboxymethyl Chitosan Nanodroplets for Combined Imaging and Synergistic Chemoradiotherapy. *Int. J. Nanomed.* **2020**, *15*, 537−552.
(169) Yu, J.; Situ, B.; Luo, M.; Li, Y.; Liao, J.; Du, M.; Cai, K.; Yang, C.; Zhang, H.; Chen, Z. Carboxymethyl-hexanoyl Chitosan Nanodroplets for Ultrasonic Imaging and Drug Delivery to Tumor. *Curr. Pharm. Des.* **2018**, *24* (15), 1682−1688.
(170) Baghbani, F.; Chegeni, M.; Moztarzadeh, F.; Mohandesi, J. A.; Mokhtari-Dizaji, M. Ultrasonic Nanotherapy of Breast Cancer Using Novel Ultrasound-Responsive Alginate-Shelled Perfluorohexane Nanodroplets: *In Vitro* and *In Vivo* Evaluation. *Mater. Sci. Eng. C* **2017**, *77*, 698−707.
(171) Zhou, X.; Guo, L.; Shi, D.; Duan, S.; Li, J. Biocompatible Chitosan Nanobubbles for Ultrasound-Mediated Targeted Delivery of Doxorubicin. *Nanoscale Res. Lett.* **2019**, *14* (1), 24.
(172) Gao, X.; Guo, D.; Mao, X.; Shan, X.; He, X.; Yu, C. Perfluoropentane-Filled Chitosan Poly-acrylic Acid Nanobubbles with High Stability for Long-Term Ultrasound Imaging *In Vivo*. *Nanoscale* **2021**, *13* (10), 5333−5343.
(173) Huebsch, N.; Kearney, C. J.; Zhao, X.; Kim, J.; Cezar, C. A.; Suo, Z.; Mooney, D. J. Ultrasound-Triggered Disruption and Self-Healing of Reversibly Cross-Linked Hydrogels for Drug Delivery and Enhanced Chemotherapy. *Proc. Natl. Acad. Sci. U. S. A.* **2014**, *111* (27), 9762−9767.
(174) Ben Daya, S. M.; Paul, V.; Awad, N. S.; Al Sawaftah, N. M.; Al Sayah, M. H.; Husseini, G. A. Targeting Breast Cancer Using Hyaluronic Acid-Conjugated Liposomes Triggered with Ultrasound. *J. Biomed. Nanotechnol.* **2021**, *17* (1), 90−99.
(175) Mancini, G. B.; McGillem, M. J. Papaverine as a Coronary Vasodilator. *Am. J. Roentgenol.* **1986**, *147* (5), 1095−1096.
(176) Kim, S. H.; Lee, H. K.; Han, M. C. Incompatibility of Water-Soluble Contrast Media and Intravascular Pharmacologic Agents. An *In Vitro* Study. *Investig. Radiol.* **1992**, *27* (1), 45−49.
(177) Zagoria, R. J.; D'Souza, V. J.; Baker, A. L. Recommended Precautions When Using Low-Osmolality or Nonionic Contrast Agents With Vasodilators. *Investig. Radiol.* **1987**, *22* (6), 513−514.
(178) Irving, H. D.; Burbridge, B. E. Incompatibility of Contrast Agents With Intravascular Medications. Work in Progress. *Radiology* **1989**, *173* (1), 91−92.
(179) Schipper, N. G. M.; Vårum, K. M.; Stenberg, P.; Ocklind, G.; Lennernäs, H.; Artursson, P. Chitosans as Absorption Enhancers of Poorly Absorbable Drugs: 3: Influence of Mucus on Absorption Enhancement. *Eur. J. Pharm. Sci.* **1999**, *8* (4), 335−343.
(180) Schipper, N. G. M.; Vårum, K. M.; Artursson, P. Chitosans as Absorption Enhancers for Poorly Absorbable Drugs. 1: Influence of Molecular Weight and Degree of Acetylation on Drug Transport Across Human Intestinal Epithelial (Caco-2) Cells. *Pharm. Res.* **1996**, *13*, 1686−1692.
(181) Kean, T.; Roth, S.; Thanou, M. Trimethylated Chitosans as Non-Viral Gene Delivery Vectors: Cytotoxicity and Transfection Efficiency. *J. Controlled Release* **2005**, *103* (3), 643−653.
(182) Flexner, C.; Barditch-Crovo, P. A.; Kornhauser, D. M.; Farzadegan, H.; Nerhood, L. J.; Chaisson, R. E.; Bell, K. M.; Lorentsen, K. J.; Hendrix, C. W.; Petty, B. G.; Lietman, P. S. Pharmacokinetics, Toxicity, and Activity of Intravenous Dextran Sulfate in Human Immunodeficiency Virus Infection. *Antimicrob. Agents Chemother.* **1991**, *35* (12), 2544−2550.
(183) Voorhees, A. B.; Baker, H. J.; Pulaski, E. J. Reactions of Albino Rats to Injections of Dextran. *Proc. Soc. Exp. Biol. Med.* **1951**, *76* (2), 254−256.
(184) Edlund, T.; LÖFgren, B.; VÄLi, L. Toxicity of Dextran in Rats. *Nature* **1952**, *170*, 125.
(185) Morrison, J. L.; Richardson, A. P.; Bloom, W. L. The Effects of Antihistaminic Agents on the Reaction of the Rat to Dextran. *Arch. Int. Pharmacodyn. Ther.* **1951**, *88* (1), 98−105.
(186) Seo, D. Y.; Jin, M.; Ryu, J.-C.; Kim, Y.-J. Investigation of the Genetic Toxicity by Dextran-Coated Superparamagnetic Iron Oxide Nanoparticles (SPION) in HepG2 Cells Using the Comet Assay and Cytokinesis-Block Micronucleus Assay. *Toxicol. Environ. Health Sci.* **2017**, *9* (1), 23−29.
(187) Sokolsky-Papkov, M.; Domb, A. J.; Golenser, J. Impact of Aldehyde Content on Amphotericin B−Dextran Imine Conjugate Toxicity. *Biomacromolecules* **2006**, *7* (5), 1529−1535.
(188) Baran, A.; Sulukan, E.; Türkoğlu, M.; Ghosigharehagaji, A.; Yildirim, S.; Kankaynar, M.; Bolat, I.; Kaya, M.; Topal, A.; Ceyhun, S. B. Is Sodium Carboxymethyl Cellulose (CMC) Really Completely Innocent? It may be Triggering Obesity. *Int. J. of Biol. Macromol.* **2020**, *163*, 2465−2473.
(189) Fan, C.; Hou, L.; Che, G.; Shi, Y.; Liu, X.; Sun, L.; Jia, W.; Zhu, F.; Zhao, Z.; Xu, M.; Gai, X.; Liu, C. Dose- and Time-Dependent Systemic Adverse Reactions of Sodium Carboxy Methyl Cellulose After Intraperitoneal Application in Rats. *J. Toxicol. Sci.* **2021**, *46* (5), 223−234.
(190) Darrah, T. H.; Prutsman-Pfeiffer, J. J.; Poreda, R. J.; Ellen Campbell, M.; Hauschka, P. V.; Hannigan, R. E. Incorporation of Excess Gadolinium into Human Bone from Medical Contrast Agents. *Metallomics* **2009**, *1* (6), 479−488.
(191) Bellin, M. F.; Van Der Molen, A. J. Extracellular Gadolinium-Based Contrast Media: An Overview. *Eur. J. Radiol.* **2008**, *66* (2), 160−167.
(192) Marckmann, P.; Skov, L.; Rossen, K.; Dupont, A.; Damholt, M. B.; Heaf, J. G.; Thomsen, H. S. Nephrogenic Systemic Fibrosis: Suspected Causative Role of Gadodiamide Used for Contrast-Enhanced Magnetic Resonance Imaging. *J. Am. Soc. Nephrol.* **2006**, *17* (9), 2359−2362.

(193) McDonald, R. J.; McDonald, J. S.; Kallmes, D. F.; Jentoft, M. E.; Murray, D. L.; Thielen, K. R.; Williamson, E. E.; Eckel, L. J. Intracranial Gadolinium Deposition after Contrast-Enhanced MR Imaging. *Radiology* **2015**, *275* (3), 772−782.
(194) White, G. W.; Gibby, W. A.; Tweedle, M. F. Comparison of Gd(DTPA-BMA) (Omniscan) Versus Gd(HP-DO3A) (ProHance) Relative to Gadolinium Retention in Human Bone Tissue by Inductively Coupled Plasma Mass Spectroscopy. *Invest. Radiol.* **2006**, *41* (3), 272−278.
(195) Di Gregorio, E.; Gianolio, E.; Stefania, R.; Barutello, G.; Digilio, G.; Aime, S. On the Fate of MRI Gd-Based Contrast Agents in Cells. Evidence for Extensive Degradation of Linear Complexes upon Endosomal Internalization. *Anal. Chem.* **2013**, *85* (12), 5627−5631.
(196) Sepúlveda, M. R.; Dresselaers, T.; Vangheluwe, P.; Everaerts, W.; Himmelreich, U.; Mata, A. M.; Wuytack, F. Evaluation of Manganese Uptake and Toxicity in Mouse Brain During Continuous $MnCl_2$ Administration Using Osmotic Pumps. *Contrast Media Mol. Imaging.* **2012**, *7* (4), 426−434.
(197) Gale, E. M.; Wey, H.-Y.; Ramsay, I.; Yen, Y.-F.; Sosnovik, D. E.; Caravan, P. A Manganese-Based Alternative to Gadolinium: Contrast-enhanced MR Angiography, Excretion, Pharmacokinetics, and Metabolism. *Radiology* **2018**, *286* (3), 865−872.
(198) Sobanska, Z.; Roszak, J.; Kowalczyk, K.; Stepnik, M. Applications and Biological Activity of Nanoparticles of Manganese and Manganese Oxides in *In Vitro* and *In Vivo* Models. *Nanomaterials (Basel)* **2021**, *11* (5), 1084.
(199) McDonald, R. J.; Levine, D.; Weinreb, J.; Kanal, E.; Davenport, M. S.; Ellis, J. H.; Jacobs, P. M.; Lenkinski, R. E.; Maravilla, K. R.; Prince, M. R.; Rowley, H. A.; Tweedle, M. F.; Kressel, H. Y. Gadolinium Retention: A Research Roadmap from the 2018 NIH/ACR/RSNA Workshop on Gadolinium Chelates. *Radiology* **2018**, *289*, 517−534.
(200) Rogosnitzky, M.; Branch, S. Gadolinium-Based Contrast Agent Toxicity: A Review of Known and Proposed Mechanisms. *Biometals* **2016**, *29*, 365−376.
(201) Yu, S. B.; Watson, A. D. Metal-Based X-ray Contrast Media. *Chem. Rev.* **1999**, *99* (9), 2353−2378.
(202) Idee, J. M.; Pines, E.; Prigent, P.; Corot, C. Allergy-Like Reactions to Iodinated Contrast Agents. A Critical Analysis. *Fundam. Clin. Pharmacol.* **2005**, *19* (3), 263−281.
(203) Dong, M.; Jiao, Z.; Liu, T.; Guo, F.; Li, G. Effect of Administration Route on the Renal Safety of Contrast Agents: A Meta-Analysis of Randomized Controlled Trials. *J. Nephrol.* **2012**, *25* (3), 290−301.
(204) Thomsen, H. S.; Morcos, S. K. Risk of Contrast-Medium-Induced Nephropathy in High-Risk Patients Undergoing MDCT − A Pooled Analysis of Two Randomized Trials. *Eur. Radiol.* **2009**, *19* (4), 891.
(205) Lee, N.; Choi, S. H.; Hyeon, T. Nano-Sized CT Contrast Agents. *Adv. Mater.* **2013**, *25* (19), 2641−2660.
(206) Leander, P.; Höglund, P.; Børseth, A.; Kloster, Y.; Berg, A. A New Liposomal Liver-Specific Contrast Agent for CT: First Human Phase-I Clinical Trial Assessing Efficacy and Safety. *Eur. Radiol.* **2001**, *11* (4), 698−704.
(207) Fu, J.-j.; Guo, J.-j.; Qin, A.-p.; Yu, X.-y.; Zhang, Q.; Lei, X.-p.; Huang, Y.-g.; Chen, M.-y.; Li, J.-x.; Zhang, Y.; et al. Bismuth Chelate as a Contrast Agent for X-ray Computed Tomography. *J. Nanobiotechnology.* **2020**, *18* (1), 110.
(208) Huang, S. D. Bismuth-Based Nanoparticles for CT Imaging. *Design and Applications of Nanoparticles in Biomedical Imaging*, Bulte, J. W. M.; Modo, M. M. J., Eds.; Springer International Publishing, 2017; pp 429−444.
(209) Towson, J. E. C.; Eberl, S. Radiation Protection and Dosimetry in PET and PET/CT. In *Positron Emission Tomography: Clinical Practice*, Valk, P. E.; Delbeke, D.; Bailey, D. L.; Townsend, D. W.; Maisey, M. N., Eds.; Springer: London, 2006; pp 41−62.
(210) Mattsson, S.; Söderberg, M. Radiation Dose Management in CT, SPECT/CT and PET/CT Techniques. *Radiat. Prot. Dosim.* **2011**, *147* (1−2), 13−21.
(211) Hicks, R. J.; Hofman, M. S. Is There Still a Role for SPECT−CT in Oncology in the PET−CT Era? *Nat. Rev. Clin. Oncol.* **2012**, *9* (12), 712−720.
(212) Mithun, S.; Jha, A. K.; Puranik, A. D.; Monteiro, P.; Shah, S.; Agarwal, A.; Purandare, N. C.; Rangarajan, V. Reduction of Radiation Exposure to Patients and Professionals by Reducing the Administered Activity of 18F-Fluorodeoxyglucose in a Positron-emission Tomography/Computed Tomography Study. *Indian J. Nucl. Med.* **2018**, *33* (1), 6−9.
(213) Delpassand, E. S.; Samarghandi, A.; Mourtada, J. S.; Zamanian, S.; Espenan, G. D.; Sharif, R.; Mackenzie, S.; Kosari, K.; Barakat, O.; Naqvi, S.; Seng, J. E.; Anthony, L. Long-Term Survival, Toxicity Profile, and Role of F-18 FDG PET/CT scan in Patients with Progressive Neuroendocrine Tumors Following Peptide Receptor Radionuclide Therapy with High Activity In-111 Pentetreotide. *Theranostics* **2012**, *2* (5), 472−480.
(214) Chitambar, C. R. Gallium and Its Competing Roles with Iron in Biological Systems. *Biochim. Biophys. Acta (BBA) − Mol. Cell Res.* **2016**, *1863* (8), 2044−2053.
(215) Rudd, S. E.; Roselt, P.; Cullinane, C.; Hicks, R. J.; Donnelly, P. S. A Desferrioxamine B Squaramide Ester for the Incorporation of Zirconium-89 into Antibodies. *Chem.Commun.* **2016**, *52* (80), 11889−11892.
(216) Vegt, E.; de Jong, M.; Wetzels, J. F. M.; Masereeuw, R.; Melis, M.; Oyen, W. J. G.; Gotthardt, M.; Boerman, O. C. Renal Toxicity of Radiolabeled Peptides and Antibody Fragments: Mechanisms, Impact on Radionuclide Therapy, and Strategies for Prevention. *J. Nucl. Med.* **2010**, *51* (7), 1049.
(217) Poland, C. A.; Duffin, R.; Kinloch, I.; Maynard, A.; Wallace, W. A. H.; Seaton, A.; Stone, V.; Brown, S.; MacNee, W.; Donaldson, K. Carbon Nanotubes Introduced into the Abdominal Cavity of Mice Show Asbestos-Like Pathogenicity in a Pilot Study. *Nat. Nanotechnol.* **2008**, *3* (7), 423−8.
(218) Pan, Y.; Neuss, S.; Leifert, A.; Fischler, M.; Wen, F.; Simon, U.; Schmid, G.; Brandau, W.; Jahnen-Dechent, W. Size-Dependent Cytotoxicity of Gold Nanoparticles. *Small* **2007**, *3* (11), 1941−1949.
(219) Zhu, M. T.; Wang, Y.; Feng, W. Y.; Wang, B.; Wang, M.; Ouyang, H.; Chai, Z. F. Oxidative Stress and Apoptosis Induced by Iron Oxide Nanoparticles in Cultured Human Umbilical Endothelial Cells. *J. Nanosci. Nanotechnol.* **2010**, *10* (12), 8584−8590.
(220) Jakobsen, J. Å.; Oyen, R.; Thomsen, H. S.; Morcos, S. K. Members of Contrast Media Safety Committee of European Society of Urogenital, R. Safety of Ultrasound Contrast Agents. *Eur. Radiol.* **2005**, *15* (5), 941−945.
(221) Mahmoudi, M.; Shokrgozar, M. A.; Sardari, S.; Moghadam, M. K.; Vali, H.; Laurent, S.; Stroeve, P. Irreversible Changes in Protein Conformation Due to Interaction with Superparamagnetic Iron Oxide Nanoparticles. *Nanoscale* **2011**, *3* (3), 1127−1138.
(222) Kedmi, R.; Ben-Arie, N.; Peer, D. The Systemic Toxicity of Positively Charged Lipid Nanoparticles and the Role of Toll-like Receptor 4 in Immune Activation. *Biomaterials* **2010**, *31* (26), 6867−6875.
(223) Shelke, N. B.; James, R.; Laurencin, C. T.; Kumbar, S. G. Polysaccharide Biomaterials for Drug Delivery and Regenerative Engineering. *Polym. Adv. Technol.* **2014**, *25* (5), 448−460.
(224) Muldoon, L. L.; Sàndor, M.; Pinkston, K. E.; Neuwelt, E. A. Imaging, Distribution, and Toxicity of Superparamagnetic Iron Oxide Magnetic Resonance Nanoparticles in the Rat Brain and Intracerebral Tumor. *Neurosurgery* **2005**, *57* (4), 785−796.
(225) Bodnar, M.; Hartmann, J. F.; Borbely, J. Preparation and Characterization of Chitosan-Based Nanoparticles. *Biomacromolecules* **2005**, *6* (5), 2521−2527.
(226) Hoskins, C.; Cuschieri, A.; Wang, L. The Cytotoxicity of Polycationic Iron Oxide Nanoparticles: Common Endpoint Assays and Alternative Approaches for Improved Understanding of Cellular Response Mechanism. *J. Nanobiotechnology.* **2012**, *10* (1), 15.

https://doi.org/10.1021/acsbiomaterials.1c01631
ACS Biomater. Sci. Eng. 2022, 8, 2281−2306

(227) Goodman, C. M.; McCusker, C. D.; Yilmaz, T.; Rotello, V. M. Toxicity of Gold Nanoparticles Functionalized with Cationic and Anionic Side Chains. *Bioconjugate Chem.* **2004**, *15* (4), 897−900.
(228) Shukla, R.; Bansal, V.; Chaudhary, M.; Basu, A.; Bhonde, R. R.; Sastry, M. Biocompatibility of Gold Nanoparticles and Their Endocytotic Fate Inside the Cellular Compartment: A Microscopic Overview. *Langmuir* **2005**, *21* (23), 10644−10654.
(229) Zhang, X. D.; Wu, H. Y.; Wu, D.; Wang, Y. Y.; Chang, J. H.; Zhai, Z. B.; Meng, A. M.; Liu, P. X.; Zhang, L. A.; Fan, F. Y. Toxicologic Effects of Gold Nanoparticles *In Vivo* by Different Administration Routes. *Int. J. Nanomedicine.* **2010**, *5*, 771.
(230) Mohammadpour, R.; Dobrovolskaia, M. A.; Cheney, D. L.; Greish, K. F.; Ghandehari, H. Subchronic and Chronic Toxicity Evaluation of Inorganic Nanoparticles for Delivery Applications. *Adv. Drug Delivery Rev.* **2019**, *144*, 112−132.
(231) Yildirimer, L.; Thanh, N. T.K.; Loizidou, M.; Seifalian, A. M. Toxicology and Clinical Potential of Nanoparticles. *Nano Today* **2011**, *6* (6), 585−607.
(232) Zhao, N.; Yan, L.; Xue, J.; Zhang, K.; Xu, F.-J. Degradable One-Dimensional Dextran-Iron Oxide Nanohybrids for MRI-Guided Synergistic Gene/Photothermal/Magnetolytic Therapy. *Nano Today* **2021**, *38*, 101118.

https://doi.org/10.1021/acsbiomaterials.1c01631
ACS Biomater. Sci. Eng. 2022, 8, 2281−2306